FGF-dependent, polarized SOS activity orchestrates directed migration of *C. elegans* muscle progenitors independently of canonical effectors *in vivo*

Theresa V Gibney[1], Jacob I Mardick[2], Neal R Rasmussen[2], Laila Latifi[1,3], Meera V Sundaram[4], David J Reiner[2,5], Ariel M Pani[1, 6, *]

[1]Department of Biology, University of Virginia, Charlottesville, VA 22903, USA.
[2]Institute of Biosciences and Technology, Texas A&M Health Science Center, Texas A&M University, Houston, TX 77030, USA.
[3]Present affiliation, Centre for Immuno-Oncology, Nuffield Department of Medicine, University of Oxford, Oxford OX3 7DQ, UK
[4]Department of Genetics, Perelman School of Medicine, University of Pennsylvania, Philadelphia, PA 19104, USA.
[5]Department of Translational Medical Science, College of Medicine, Texas A&M Health Science Center, Texas A&M University, Houston, TX 77030, USA.
[6]Department of Cell Biology, University of Virginia School of Medicine, Charlottesville, VA 22903, USA
* lead contact, amp2na@virginia.edu

Summary

Directed cell migration is essential for animal development, tissue maintenance, regeneration, and disease states. Cells often migrate towards, or away from, sources of secreted signaling proteins that impart spatial information. How migrating cells interpret extracellular signals to orient and navigate within living animals is a fundamental question in biology. Receptor Tyrosine Kinase (RTK) signaling plays critical roles in cell migration, and aberrant RTK pathway activity is a key driver of multiple types of cancers. Yet, how RTKs control cell migration in living animals remains unclear, in part due to essential, pleiotropic roles of key proteins in development. To elucidate how RTK signaling controls cell migration *in vivo*, we used *C. elegans* muscle progenitor migration as a tractable system to dissect spatial and temporal requirements for key signal transduction and cytoskeletal regulatory proteins. Cell type-specific depletion of endogenously tagged proteins revealed that homologs of FGFR, GRB2, SOS, and Ras control cell migration independent of their canonical ERK, PI3K, AKT, mTOR, and PLCγ effectors. Instead, we found that FGF-dependent, polarized SOS-1 orients migrating cells towards an FGF source, and mislocalizing SOS activity within migrating cells severely disrupts migration independent of ERK. Cell type-specific gain-of-function experiments demonstrated that activated Ras/LET-60 acts permissively in this context, and an intragenic revertant identified in a screen for suppressors of activated *Ras/let-60* revealed that signal transduction in migrating muscle progenitors can be genetically uncoupled from other Ras-dependent developmental processes. Our findings provide a novel mechanism for RTK-directed cell migration *in vivo* and highlight the importance of cell type-specific approaches to elucidate signal transduction mechanisms in physiologically relevant contexts. Our work also outlines a comprehensive framework for investigating RTK-dependent processes in a multicellular organism and introduces a versatile genetic toolkit for dissecting spatial and temporal signaling dynamics fundamental to development, homeostasis, and disease

Introduction

Directed cell migration is a fundamental process in animal development and allows integrated organ systems to be assembled from disparate cell lineages born from distant progenitors[1,2]. Migrating cells often rely on positional information from extracellular ligands to precisely navigate through the complex and dynamic environment of a developing animal to reach their destinations[1–3]. To do so, cells must translate extracellular cues that impart spatial information about their surroundings into coordinated cytoskeletal rearrangements that drive directional cell motility[2,4]. Receptor Tyrosine Kinases (RTKs) are a prominent, evolutionarily conserved class of transmembrane receptors that bind growth factors and other extracellular signaling molecules[5]. Signaling through RTKs is essential for developmental and homeostatic processes including cell migration, proliferation, differentiation, and survival, and abnormal RTK pathway activation is implicated in cancer and congenital disorders[5–7]. Canonical RTK activation leads to recruitment of cytosolic adaptor and effector proteins such as Growth factor Receptor-Bound protein 2 (GRB2), which recruits Son-of-Sevenless (SOS; SOS-1 in *C. elegans*), which in turn activates small GTPases including Ras and Rac and their associated signal transduction pathways[5,8]. RTK signal transduction can involve multiple downstream effector pathways, including ERK/MAP Kinase, PI3K, Akt, mTORC1, and PLCγ, which allows diverse functions for individual receptors in different contexts[5,9,10].

Fibroblast Growth Factors (FGFs) are a class of secreted signaling proteins that play critical roles in animal development and tissue maintenance, can disperse between cells over long distances, and can convey spatial information[11–13]. At the cellular level, FGFs act through their RTK FGF Receptors (FGFRs) to regulate cell behaviors such as migration along with other processes including proliferation and patterning[14–16]. While FGF signaling is required for cell migration in multiple contexts during animal development[17–20], methodological challenges and pleiotropy have hampered dissecting the signal transduction mechanisms by which FGFs guide migrating cells *in vivo*. In particular, essential roles for key proteins in other aspects of development or physiology have confounded efforts to investigate their roles in cell migration using genetic methods. Consequently, our current understanding of the cell biological mechanisms by which extracellular cues such as FGFs direct cell migration comes largely from experiments in unicellular organisms and cultured cell systems, which are experimentally tractable but devoid of the developmental and organismal contexts that govern cell migration *in vivo*[21,22]. Investigations of how RTK and/or Ras signaling regulate cell migration in cultured cells and unicellular models for cell motility have revealed roles for Ras, MAPK, and PI3K activity in recruiting Rac-GEFs, the ARP2/3 complex, WAVE, and WASP proteins that can organize local actin polymerization in response to RTK signaling[4,23]. In animals, FGFs may also control cell migration through transcriptional mechanisms rather than by directly influencing cell behavior[24–26]. Despite conserved roles for FGF and RTK signaling in cell migration and their importance in disease states, we lack a clear understanding of the signal transduction processes that translate positional information encoded by extracellular FGF into directional cell migration in living animals. Dissecting these mechanisms will require the ability to visualize migrating cell dynamics and to manipulate key endogenous proteins *in vivo* with spatial and temporal precision to bypass pleiotropic effects.

C. elegans postembryonic muscle progenitors provide an experimentally tractable framework to dissect cell signaling mechanisms in a living animal. During early larval development, two muscle progenitors, the sex myoblasts (SMs), migrate anteriorly from their birthplace near the tail and stop over the dorsal uterine cells located at the center of the developing gonad. There, SMs proliferate and differentiate into vulval and uterine muscle cells essential for egg-laying[27,28]. The FGF8/17/18 family homolog EGL-17 is a diffusible chemoattractant that acts instructively to guide migrating SMs[29–31]. FGF/EGL-17 is secreted by ventral midline blast cells during early SM migration, followed by high expression in the primary (1°) vulval precursor cell (VPC), and uterine cells[31]. Loss of FGF/EGL-17 or the 5a isoform of FGFR/EGL-15 results in migration failure and posterior displacement of SMs[27,32]. FGF or FGFR loss of function does not affect SM proliferation or cell fates at this stage, thereby making these cells a powerful system to separate mechanisms of signal transduction that direct cell migration from those involved in other FGF-dependent processes. Prior work has explored the role of canonical RTK-Ras-ERK signaling in SM migration[10,33], but these studies were historically constrained to using missense mutations or mosaic analyses, as complete loss of function for critical genes in this pathway confers early larval lethality[33]. Mutant analyses for many key proteins are also confounded by pleiotropic effects, such as roles for Ras-ERK signaling in fate specification of FGF-expressing cells that attract migrating SMs[34–36]. Current data indicate the Ras homolog *let-60* is required for SM migration, but may act permissively, while roles for other signal transduction pathways that act downstream of RTKs including PI3K-Akt-mTOR and PLCγ have not been reported[1,33]. Likewise, the signal transduction mechanisms that are responsible for orienting migrating SMs towards an extracellular FGF source are unknown.

To address these fundamental questions about how spatial information provided by a diffusible FGF is translated into directed cell migration towards the FGF source, we systematically tested functions for candidate proteins with potential roles in RTK-mediated cell polarization and motility *in vivo*. We used temporal and cell type-specific depletion of tagged endogenous proteins to interrogate spatial and temporal roles of sixteen core signal transduction and cytoskeletal regulatory proteins with plausible roles in FGF-directed cell migration. Surprisingly, we found that canonical RTK effectors including homologs of ERK, PI3K, Akt, mTOR, and PLCγ, are dispensable for SM migration *in vivo*. Unexpectedly, we identified polarized SOS-1 activity as a key link between extracellular FGF and directed cell migratory behaviors independent of its known functions in activating ERK or Rac. In migrating SMs, tagged endogenous SOS-1 localized to the cell membrane in an FGFR-dependent manner and is polarized towards cells that express FGF/EGL-17. Uniformly activating SOS around the cell membrane disrupted FGF-directed cell migration through an ERK-independent mechanism and led to cell migration defects resembling loss of SOS-1 function. While polarized SOS activity was required to orient migrating SMs, activated alleles of Ras/LET-60 acted permissively rather than instructively in this context. Moreover, an intragenic revertant allele of an activating mutation in *Ras/let-60* genetically separated the function of *Ras/let-60* in SM migration from its ERK-dependent roles in larval viability and VPC cell fate specification. These findings challenge prevailing views on RTK signal transduction in cell migration, offer a mechanism for how FGF signaling guides cell migration in a developing animal, and provide a novel toolkit to dissect RTK signal transduction and cytoskeletal regulation *in vivo*.

RESULTS

An FGFR-GRB2-SOS-Ras module regulates SM migration

To test functions for candidate proteins in SM migration, we used Cas9-triggered homologous recombination to tag endogenous proteins with an auxin-inducible degron (AID) that targets AID-tagged proteins for degradation in the presence of an exogenous TIR1 adaptor protein and the small molecule auxin or its analog K-NAA[37,38] (Figure 1A). To deplete proteins of interest in migrating SMs, we expressed TIR1 using an *hlh-8/twist* promoter[39] that drives strong expression in the post-embryonic M lineage before, during, and after SM migration[40]. Using this approach, we tagged and depleted endogenous proteins hypothesized to act in FGF signal transduction or to be required for FGF-mediated migration.

We first investigated functions for five core components of the FGFR-Ras-ERK pathway (Figure 1C), which were previously implicated in SM migration based on mutant analyses[33]. Mutations in the *5a* isoform of *egl-15,* the sole *C. elegans* FGF receptor, severely disrupt SM migration, which also requires the FGF ligand EGL-17 [30,32,41] (Figure 1B). *Ras/let-60* was previously implicated as a permissive signal for FGF-dependent SM migration using mosaic rescue analyses[33], but attempts to elucidate the mechanisms that orient SM migration towards an FGF source have been complicated by pleiotropic effects of key candidate genes. To determine how cells translate an extracellular FGF signal into directed migratory behaviors, we endogenously tagged homologs of FGF Receptor (FGFR/EGL-15), Growth factor Receptor-Bound protein 2 (GRB2/SEM-5), Son of Sevenless (SOS/SOS-1), Ras (Ras/LET-60), Kinase Suppressor of Ras (KSR/KSR-1), and Extracellular signal Regulated Kinase 1/2 (ERK/MPK-1) to visualize their localization and allow for cell type-specific protein depletion. FGFR/EGL-15::mNG::AID, GRB2/SEM-5::mScarlet-I::AID, mNG::AID::SOS-1, mNG::AID::KSR-1, and mNG::AID::ERK/MPK-1 knock-in animals appeared wild-type in the absence of the auxin analog K-NAA. We observed larval lethality for mScarlet-I::AID::LET-60 similar to that previously observed with an mNG::LET-60 tag[42]. However, we successfully generated separate, biologically functional mScarlet-I::LET-60 and AID::LET-60 knock-ins using an extended 30 amino acid flexible linker.

To assess functions for these proteins in SM migration, we depleted AID-tagged endogenous proteins using a *Phlh-8*-driven transgene that expresses TIR and a plasma membrane marker in M lineage cells. We treated with K-NAA or vehicle (water) and scored SM position at the early L3 stage based on proximity to the central P6.p-P8.p VPCs as well as the M-lineage-derived body wall muscles (Figure S1). To validate our cell type-specific depletion approach, we first depleted FGFR/EGL-15, which led to strong SM migration defects (Figure 1D,E) that phenocopied *egl-15(n1458),* which is a presumptive null mutation in the *egl-15(5a)* isoform required for SM migration[43]. Depleting the RTK adaptor protein GRB2/SEM-5 in SMs using *Phlh-8*-driven TIR1 resulted in migration defects similar to FGFR depletion, consistent with a requirement for GRB2/SEM-5 in FGFR/EGL-15 signal transduction. Depleting the guanine nucleotide exchange factor SOS-1 or its small GTPase substrate Ras/LET-60 led to similar, although slightly less penetrant, defects in SM migration consistent with essential functions for these proteins downstream of activated FGFR (Figure 1D,E).

Strikingly, we did not observe SM migration defects upon depletion of either KSR-1 or ERK/MPK-1 in the M lineage (Figure 1D, E), suggesting these proteins are not cell-autonomously essential for FGF signal transduction during SM migration. To rule out the possibility of insufficient KSR-1 degradation, we examined SM migration in animals carrying a *ksr-1(n2526)* mutation, which introduces a premature stop codon that truncates KSR-1 before its catalytic domain. While two missense alleles of *ksr-1* were reported to cause moderate SM migration defects[33], we observed normal SM positioning in *ksr-1(n2526)* null mutants, which corroborated the results of our cell type-specific KSR-1 depletion (Figure S2A, B). Although *ksr-1* sometimes acts redundantly with *ksr-2*, L2 stage scRNAseq data[44] indicate that *ksr-2* is not normally expressed in SMs. ERK/MPK-1 is an essential gene that has pleiotropic roles in specifying the fates of FGF/EGL-17-producing cells that attract migrating SMs[45,46], which has complicated testing its functions in SM migration using mutants. We validated that our mNG::AID::MPK-1 allele was capable of imposing strong loss of function using a ubiquitously expressed *Prpl-28>TIR1* transgene to deplete ERK/MPK-1 in all cell types. Whole-body depletion of mNG::AID::MPK-1 phenocopied the fully penetrant adult sterility and larval lethality of *mpk-1* null mutants indicating that mNG::AID::ERK/MPK-1 depletion is capable of replicating the most severe loss of function phenotypes. While we did not observe migration defects in ERK/MPK-1-depleted SMs, we observed unusually long and thin cells (Figure S3). This observation validated depletion of ERK/MPK-1 while also implying that ERK/MPK-1 performs roles in SMs other than migration. Taken together, our cell type-specific depletion experiments demonstrated that the conserved FGFR-GRB2-SOS-Ras signaling module regulates SM migration, likely independent of ERK/MPK-1, which acts downstream of RTK-Ras signaling in many other contexts[10].

SM migration does not require PI3K, Akt, mTOR, or PLCγ activity

As ERK/MPK-1 was not required in the M lineage for SM migration, we next tested functions for the PI3K-Akt pathway (Figure 2A). PI3K-Akt signaling can mediate ERK-independent signal transduction downstream of Ras[9,23], and is required for chemoattractant-driven migration in *Dictyostelium*[4,22]. To target PI3K-Akt signaling, we generated functional, mNG::AID-tagged alleles of the PI3K catalytic subunit AGE-1, the homolog of its downstream signaling effector Akt/PKB/AKT-1, and the mTOR homolog LET-363 (Figure 2A). Because *C. elegans* encodes two *akt* homologs that typically act redundantly[47], we generated AKT-1::mNG::AID in the viable *akt-2(ok393)* null mutant background. Depletion of PI3K/AGE-1 or AKT activity in the SMs had no effect on SM migration (Figure 2B,C). To validate effective depletion via our AID-tagged alleles, we depleted the tagged endogenous proteins throughout the animal using ubiquitously expressed TIR1. Strong *age-1* or *akt-1; akt-2* null mutants exhibit a maternal effect, constitutive dauer phenotype in the F2 generation[47]. Whole body depletion of AGE-1::mNG::AID or AKT-1::mNG::AID; *akt-2(ok393)* led to 100% F2 dauer progeny, which phenocopied putative null phenotypes and validated strong loss of function using our methodology.

Given the importance of PI3K-Akt signaling in cell migration in other contexts, we sought to independently confirm that PI3K signaling is not required for SM migration. F1 generation *age-1(m333)* homozygotes from heterozygous mothers are reported to be egg-laying deficient[48],

which is a classic phenotypic outcome of SM migration defects[30]. Since the dauer phenotype of *age-1(m333)* null mutants occurs in the F2 generation, we examined SM positioning in F1 progeny of balanced *age-1(m333)/*mnC1 animals, which are expected to be 1/3 homozygous and 2/3 heterozygous for the *age-1(m333)* mutation (mnC1 homozygotes are Dpy Unc). Interestingly, we observed an M lineage defect that affected SM differentiation in 6.5% of the total worms analyzed (equivalent to 19% of the predicted homozygous *age-1(m333)* animals) (Figure S2C; Table S1). However, we observed no SM migration defects in animals with normal M lineage differentiation. These findings confirmed PI3K signaling is not required for SM migration while *age-1* has earlier functions in M lineage differentiation, likely through non-cell-autonomous activity. To test the possibility that ERK and PI3K act redundantly in SM migration, we simultaneously depleted AGE-1::mNG::AID and mNG::AID::ERK/MPK-1 in the M lineage. SMs migrated normally in most animals (Figure 2B,C). We also observed thinner SMs in AGE-1; MPK-1 depleted animals (Figure 2C), consistent with the phenotype caused by ERK/MPK-1 depletion alone. We next evaluated the consequences of depleting the mTOR homolog LET-363, a protein that acts downstream of PI3K-Akt and promotes cell migration in contexts including cancer metastasis and T cell migration[49]. M lineage-specific depletion of mNG::AID::LET-363/mTOR in early larval development led to a striking phenotype where M lineage cells were entirely absent in many animals at the L3 stage. In animals where M lineage cells were visible, they were drastically smaller than normal, and SMs failed to migrate (Figure 2D). To test the extent to which mTOR/LET-363 directly regulates SM migration, we delayed K-NAA addition until after the SMs were born, but several hours before the onset of FGF-dependent migration. We did not observe migration defects with timed mTOR/LET-363 depletion, although SMs were still smaller when compared to control animals (Figure 2E). Overall, our results suggest that PI3K, AKT, and mTOR signaling are not cell-autonomously required for SM migration, and that the PI3K-Akt and ERK pathways do not act redundantly in this process.

FGFs can also regulate cell migration through activation of Phospholipase-C gamma (PLCγ), which can in turn signal through Ca^{2+}, diacylglycerol, and Protein Kinase C (PKC) family proteins[50–52]. The single *C. elegans* PLCγ homolog, PLC-3, acts downstream of EGFR/LET-23 in gonadal sheath cells and the ALA neuron[53,54], suggesting that *C. elegans* RTKs are similarly capable of signaling through PLCγ. PLC-3 null mutants are sterile and thus may not have been identified in genetic screens to identify egg-laying deficient animals. To test functions of PLCγ in SM migration, we imaged SM positioning in homozygous *plc-3(tm1340)* offspring of heterozygous *plc-3(tm1340)/+* parents. SM positioning was unaltered in these *plc-3* mutants (Figure S2D), indicating this pathway does not play an essential role in SM migration.

Extracellular FGF/EGL-17 orients SOS-1 localization in migrating cells

To understand how migrating SMs navigate towards an FGF source, we next sought to determine the extent to which GRB2/SEM-5, SOS/SOS-1, and Ras/LET-60 act instructively to orient migrating cells versus permissively to allow migration. We first examined subcellular localization of the endogenously tagged proteins during the FGF-dependent phase of SM migration[27]. SOS and GRB2 homologs are cytosolic proteins that are recruited to the cell membrane by activated growth factor receptors, whereas Ras proteins are membrane-anchored

through prenyl lipid modification of a C-terminal CAAX domain[55,56]. Strikingly, we found that mNG::AID::SOS-1 punctae localized to the cell membrane along the leading and ventral edges of migrating SMs (Figure 3A), which face the somatic gonad and ventral midline cells that express FGF/EGL-17 at this stage[31]. Time-lapse imaging revealed that mNG::AID::SOS-1 localized to dynamic punctae within active leading-edge protrusions in migrating SMs (Figure 3B; Video 1), suggesting these locations are sites of receptor activation. GRB2/SEM-5::mScarlet-I::AID localized to sparse punctae at the cell membrane and faintly in the cytoplasm of migrating cells (Figure 3C), but the protein was expressed at low levels and photobleached rapidly. Ras/mScarlet-I::LET-60 localized primarily to the plasma membrane without obvious anteroposterior polarization and was also visible in larger intracellular punctae (Figure 3D). To assess the possibility that SOS-1 translates the direction of an FGF source into a polarized intracellular signal, we first tested the extent to which SOS-1 localization in SMs responds to FGF signaling. Membrane localization of mNG::AID::SOS-1 was lost in the FGFR mutant *egl-15(n1458),* indicating that of SOS-1 localization to the SM membrane depends on FGFR/EGL-15(5A) (Figure 3E). To test the extent to which subcellular SOS-1 localization provides an intracellular readout of the position of an extracellular FGF source, we deleted the FGF homolog (EGL-17) required for SM migration and then misexpressed FGF/EGL-17 in a small cluster of posterior cells using a fragment of the *egl-20* promoter to reorient SM migration towards the tail[31]. In *FGF/egl-17(⊿); Pegl-20>FGF/egl-17* animals, we observed that mNG::AID::SOS-1 punctae localized to the posterior end of SMs as they migrated towards the tail (Figure 3F), consistent with an instructive role for SOS-1 in directing SM migration towards FGF-expressing cells.

SOS-1 provides a directive cue for SM migration

As SOS-1 is required cell-autonomously for SM migration, and subcellular localization of mNG::AID::SOS-1 reflects the direction of an FGF source, we sought to test the possibility that polarized SOS activity is essential to orient migrating SMs. Alternatively, SOS-1 may be permissively required for SM migration but not responsible for the ability of SMs to navigate towards an FGF source. To test if asymmetric SOS activity is required for directed SM migration, we forced uniform SOS activity around the cell membrane using a SOS catalytic domain[57] (SOS^{cat}) fused to 2x mTurquoise2 (mT2) and the pleckstrin homology (PH) domain of *plc1δ1*, which associates with the inner leaflet of the plasma membrane[58] (Figure 4A). Expressing SOS^{cat}::2x mT2::PH in the M lineage arrested SM migration in a wild-type background, although the phenotype was less penetrant than depletion of SOS-1 or FGFR (Figure 4B, E). Intriguingly, SOS^{cat}::2x mT2::PH expression also resulted in dorsal displacement of 16% of SMs, which is approximately triple the incidence of dorsoventral defects seen in *FGFR/egl-15(n1458)* animals (Figure 4E, Table S1). *Phlh-8*>SOS^{cat}::2x mT2::PH also prevented SMs from migrating towards an ectopic, posterior FGF source in *FGF/egl-17* null animals with *FGF/egl-17* expressed near the tail (Figure 4C, E), further validating that asymmetric SOS activity is required for SMs to migrate towards an FGF source, regardless of direction.

To rule out the possibility that SOS^{cat}::2x mT2::PH arrests SM migration through hyperactivating ERK, we used auxin-inducible degradation to deplete endogenous mNG::AID::ERK/MPK-1 in SMs in *Phlh-8*>SOS^{cat}::2x mT2::PH animals. Intriguingly, ERK/MPK-1 depletion in SMs

suppressed the dorsal migration defects caused by SOS^{cat}::2x mT2::PH but enhanced the anterior migration defects (Figure 4D, E). This result suggests that increased ERK activity in SOS^{cat}::2x mT2::PH SMs can partially rescue their ability to migrate anteriorly, although ERK/MPK-1 is not required in the SMs for their normal migration. To investigate how uniform SOS^{cat} localization impaired SM migration, we visualized actin in *Phlh-8*>SOS^{cat}::2x mT2::PH animals using 2x mKate2 fused to a *moesin* actin-binding domain[59]. In many types of migrating cells, including SMs, actin is enriched in protrusions at the leading edge[31,60]. However, in *Phlh-8*> SOS^{cat}::2x mT2::PH animals, we observed aberrant, actin-rich protrusions around the periphery of the cell at the point where migration failed (Figure 4F). These findings suggest that uniform SOS^{cat} activity around the cell membrane disrupts cell migratory behavior by altering cytoskeletal dynamics.

Because GRB2 typically links SOS to activated growth factor receptors[55], we next tested the extent to which subcellular GRB2/SEM-5 polarization is also required for SM migration. In an attempt to uniformly target GRB2/SEM-5 to the cell membrane without disrupting its function, we used the *hlh-8* promoter to express a modified version of SEM-5::mNG with its SH2 domain replaced with the *plc1δ1* PH domain (Figure S4A). This transgene disrupted migration in approximately 15% of SMs, which may be attributable to its only weak membrane localization (Figure S4B, C) compared to SOS^{cat}::2x mT2::PH. In *Phlh-8*>SEM-5::PH::mNG animals, approximately half of cells with anterior migration defects also exhibited dorsal displacement similar to the increased frequency of dorsal migration defects with uniform SOS^{cat} localization.

Activated Ras/LET-60 acts permissively in SM migration

Next, we investigated the extent to which Ras/LET-60 functions as a permissive versus directive signal for FGF-directed SM migration. SM positioning was previously shown to be normal in *let-60(n1046[G13E])* gain of function mutants, and *n1046[G13E]* can rescue anterior SM migration in the absence of FGF signaling, which suggested a permissive role for *Ras/let-60*[33]. However, cell autonomous functions for activated Ras alleles have not been tested. To determine the effect of constitutively active Ras in the context of cell type-specific gain of function, we used the *hlh-8* promoter to express a gain-of-function *let-60(G13E)* allele in wild-type and *FGFR/egl-15(n1458)* mutant animals. Similar to *let-60(n1046)* gain of function mutants, *Phlh-8>let-60(G13E)* partially rescued SM migration in *egl-15(n1458)* mutants (Figure 5A, C), but led to prominent dorsoventral migration defects (Figure 5A,C; Table S1). In contrast to the migration defects caused by SOS^{cat}::2x mT2::PH, expressing activated LET-60(G13E) in SMs did not perturb their migration in a wild-type background (Figure 5A, C). Together, these findings suggest that polarized SOS activity orients migrating SMs towards FGF while an activated Ras allele acts permissively in their migration.

To test the extent to which SM-specific *Ras/let-60(G13E)* expression rescues SM migration through mechanisms distinct from its ERK-independent role in SM migration, we depleted mNG::AID::ERK/MPK-1 in the M lineage in *FGFR/egl-15(n1458); Phlh-8>Ras/let-60(G13E)* animals. ERK/MPK-1 depletion partially suppressed the ability of activated *Ras/let-60(G13E)* to rescue SM migration in the *FGFR/egl-15(n1458)* background (Figure 5C; Figure S5) and more strongly suppressed the dorsal SM migration defects observed in *FGFR/egl-15(n1458); Phlh-*

8>Ras/let-60(G13E) animals from 29% of cells to 4% (Figure 5C). These findings suggest that activated *Ras/let-60(G13E)* can promote SM migration cell autonomously through an ERK-dependent mechanism that differs from the function of wild-type Ras/LET-60 and highlights the ability of a single protein to modulate cell migration through multiple pathways.

The role for Ras/LET-60 in SM migration is genetically separable from canonical Ras-ERK-dependent developmental processes

As Ras/LET-60 is required cell-autonomously for SM migration, but overactivation does not confer a phenotype in a wild-type background, we hypothesized that SM migration may be genetically separable from other developmental processes that require Ras/LET-60. We turned to unpublished intragenic revertant mutations in *let-60(n1046gf)* that were identified in a screen for suppressors of activated *Ras/let-60.* Mutations identified in this manner defined much of the signal transduction pathway downstream of Ras in *C. elegans*[10]. One intragenic revertant, *let-60(n1046ku75)* suppressed the multivulval phenotype of *let-60(n1046)* and selectively impaired SM migration relative to other developmental processes. SM migration defects were observed in 93% of *let-60(n1046ku75)* animals with only minimal effects on larval survival and vulval induction (Table S2). *ku75* is a point mutation in *let-60(n1046)* that causes a Glycine>Aspartic acid substitution at amino acid position 75 (G75D) in the switch II region of Ras/LET-60 (Figure 5B; Figure S6), which is predicted to interfere with binding to SOS-1 (Figure S7; Video S1). To eliminate the possibility that linked mutations affecting other genes might underlie the SM migration phenotype in *let-60(n1046ku75)* animals, we used co-CRISPR to generate a new *let-60(G13E)* allele in an unmutagenized background followed by a second co-CRISPR genome edit to generate *let-60(G13E G75D)* animals. Similar to the intragenic revertant mutation, CRISPR-edited *let-60(G13E G75D)* suppressed the multivulval phenotype caused by *let-60(G13E)*[35,36] without noticeable larval lethality or early developmental abnormalities (Figure 5D, E). We observed SM migration defects in the majority of genome edited *let-60(G13E G75D)* animals (Figure 5C), confirming that the combination of G13E and G75D substitutions more severely disrupts *Ras/let-60* activity in SM migration compared to its essential, ERK-dependent functions in other aspects of development.

Many cytoskeletal regulators are individually dispensable for SM migration

Given our findings that GRB2/SEM-5, SOS/SOS-1, and Ras/LET-60 are required cell-autonomously for SM migration, we next sought to identify downstream proteins linking these signal transduction components to the cytoskeletal remodeling required for directed cell migration. Because SMs migrate with broad, actin-rich protrusions at the leading edge[31], we focused on cytoskeletal regulatory proteins with known roles in crawling cell motility[61–64]. We generated biologically functional, endogenous fluorescent protein::AID-tagged alleles for homologs of Rac (CED-10), RhoG (MIG-2), ARP2 (ARX-2), WAVE (WVE-1), WASP (WSP-1), and ROCK (LET-502). We also tagged the homolog of the non-receptor tyrosine kinase Abl (ABL-1), which mediates the Rac-GEF activity of vertebrate SOS proteins[65,66]. Studies in mammalian cell culture and in *Dictyostelium* have implicated homologs of Rac, the Arp-2/3 complex, WAVE, and WASP as downstream effectors that can link Ras to directed cell migration[67,68]. Given the ability of SOS proteins to directly activate Rac[8,66] and established roles for Rac in cell migration[69], we first interrogated functions for Rac/CED-10 and RhoG/MIG-2,

which acts redundantly or in parallel with CED-10 in many contexts[63,70]. *ced-10* and *mig-2* mutations do not affect SM migration individually, and *ced-10; mig-2* compound mutants have numerous developmental abnormalities including major defects in vulval development[70]. Depleting Rac/CED-10 plus RhoG/MIG-2 in the M lineage resulted in variable phenotypes including defects in cell division orientation (Figure 6B) and fate determination that precluded identifying specific roles in SM migration. To circumvent earlier defects, we treated synchronized larvae with K-NAA immediately after the SMs were born to deplete Rac/CED-10 and RhoG/MIG-2 during migration using the same strategy as for timed mTOR/LET-363 depletion (Figure 6E; Figure S8; Table S1). Simultaneously depleting mScarlet-I::AID::CED-10 and mNG::AID::MIG-2 after SM birth led to mild migration defects in approximately 10% of animals (Figure 6E; Figure S8), suggesting Rac/RhoG activity contributes to normal migration but is redundant with other mechanisms. Continuous depletion of ARX-2::mNG::AID, WVE-1::mNG::AID, or WVE-1::mNG::AID plus WSP-1::mNG::AID in the M lineage caused similar developmental defects including abnormal cell division patterns (Figure 6C, D). However, depleting ARX-2::mNG::AID, WVE-1::mNG::AID, and WVE-1::mNG::AID plus WSP-1::mNG::AID after SM birth had no effect on SM migration (Figure 6E; Figure S8). We did not observe abnormalities in M lineage development or SM migration after continuously depleting ROCK/mNG::AID::LET-502 or ABL-1::mNG::AID in the M lineage (Figure 6E; Figure S8). SMs also migrated normally in *abl-1(ok171)* null mutant animals (Figure S2), confirming that ABL-1 does not mediate the essential function of SOS-1 in SM migration. Taken together, our results suggest considerable redundancy in functions for key cytoskeletal regulators during SM migration and highlight the ability of cells to migrate accurately in the absence of key cytoskeletal regulatory proteins[71].

Discussion

RTKs regulate cell migration in many contexts during animal development, and aberrant RTK activity drives cancer and other disease states[5,72,73]. Yet, elucidating the underlying cellular and molecular mechanisms that orient migrating cells downstream of RTKs in living animals has been challenged by pleiotropy and a lack of systematic approaches to dissect functions in cell migration without perturbing other critical developmental or physiological processes. Here, we used cell type-specific depletion of 16 endogenously tagged proteins to test functions for key signal transduction and regulatory proteins in the migration of *C. elegans* postembryonic mesoderm progenitors. Our results provide a novel mechanism by which migrating cells orient towards an extracellular growth factor source and raise new questions about how RTK signal transduction directs cell migration in living animals. Surprisingly, we found that homologs of FGFR, GRB2, SOS, and Ras were required for SM migration towards an FGF source, but key downstream effectors in the ERK, PI3K-Akt-TOR, and Rac/Rho families were not required cell-autonomously. Instead, our work demonstrated that FGFR-dependent, localized SOS activity orients migrating SMs towards an FGF source independent of canonical RTK effectors. We found that SOS is localized at the leading edge of migrating SMs and provides an intracellular readout of the direction of an FGF source. Uniform SOS^{cat} localization at the cell membrane disrupted polarized protrusive behaviors in migrating SMs and prematurely arrested SM migration. The function of SOS^{cat} did not depend on ERK in this context, and simultaneous ERK/MPK-1 depletion in fact enhanced migration defects in SOS^{cat}::2x mT2::PH cells. As FGFs

and other growth factors provide positional information in developing animals and regulate cell migration in multiple systems, our findings may be broadly applicable towards understanding the cell biological mechanisms by which FGFs and RTKs orchestrate critical aspects of animal development.

Ras and Rac family proteins are thought to be the primary targets activated by SOS[8,10,75]. This hypothesis is supported by the finding that Ras/LET-60 depletion results in SM migration phenotypes similar to SOS-1 depletion. However, while we found clear evidence that SOS functions as an instructive directional cue for FGF-directed SM migration, our results are most consistent with a model where Ras/LET-60 acts permissively in this context. Endogenous Ras/LET-60 protein is not obviously polarized in migrating SMs, *Ras/let-60(G13E)* gain of function mutants do not have defects in SM migration, expressing activated *Ras/let-60(G13E)* in migrating SMs does not affect SM migration in a wild-type background, and *Ras/let-60(G13E)* expression can cell autonomously rescue SM migration in an *FGFR/egl-15(5a)* mutant. However, differences in the signal transduction mechanisms downstream of wild-type Ras/LET-60 and an activated G13E allele in SMs complicate inferring the mechanisms used in wild-type migration based on gain of function conditions. Ras activity may also be polarized, even if the protein is not, and we cannot rule out the possibility that Ras/LET-60 activity is localized within migrating cells, including in gain of function mutants. In the future, biosensors for subcellular Ras activation that do not require overexpression of Ras-binding proteins may be informative to determine the extent to which Ras activity is polarized in migrating SMs. Current methods also do not allow for selective activation of Ras at the subcellular level without manipulating Ras-GEFs such as SOS. If such techniques are developed in the future, they will provide valuable insights into the mechanisms by which Ras/LET-60 mediates SM migration.

Interestingly, we observed that depletion of SOS-1 and Ras/LET-60 leads to a slightly less penetrant SM migration phenotype compared to FGFR/EGL-15 or GRB2/SEM-5 depletion, suggesting that another effector may operate downstream of GRB2/SEM-5 in addition to SOS-1. GRB2 family proteins are adapters that recruit SOS family proteins to activated RTKs, but SOS-1 and GRB2/SEM-5 exhibit distinct localization patterns during SM migration. While mNG::AID::SOS-1 forms dynamic punctae in the leading edge protrusions of migrating SMs, GRB2/SEM-5::mNG::AID does not, with the caveat the GRB2/SEM-5::mScarlet-I::AID is expressed at low levels in SMs and photobleaches rapidly. Yet, attempts to uniformly localize GRB2/SEM-5::mNG to the plasma membrane did result in cell migration defects with low penetrance, suggesting that polarized activity of GRB2/SEM-5 may play a role in SM migration. Although there is not genetic evidence for proteins other than SOS-1 acting downstream of GRB2/SEM-5 in the context of SM migration, this system could provide a valuable model for identifying additional GRB2/SEM-5-binding proteins that may be implicated in RTK-dependent, directed cell migration.

Our investigation also revealed a novel genetic interaction between two mutations in *Ras/let-60*, G13E and G75D, that offers insights into cell type-specific signal transduction mechanisms downstream of an activating mutation in *Ras/let-60*. Ras family proteins are highly conserved in animals and play crucial roles in fundamental cellular processes including survival, proliferation,

and migration[7,10,76]. Strong *Ras* gain-of-function mutations are a major driver of tumorigenesis and metastasis while other types of mutations result in a spectrum of diseases called RASopathies[7,76,77]. The intragenic revertant allele *Ras/let-60(G13E G75D)* described here demonstrates that the ERK-dependent, essential roles for *Ras/let-60* in larval viability and VPC fate specification are genetically separable from its function in SM migration. The mechanism by which the *Ras/let-60(G13E G75D)* allele differentially affects SM migration is unknown but could involve interactions with GEFs, modulators such as Ras-GAPs, or downstream effectors. Substitutions at amino acid 75 are expected to result in reduction of function based on saturation mutagenesis assays[78], and the classical *let-60(n2021)* mutant is a G75S substitution that functions as a moderate loss of function allele[35]. Intriguingly, amino acid 75 is located in the Ras switch II domain, which plays a crucial role in tight binding of Ras to SOS[79,80], and the G75D substitution is predicted to affect interactions between Ras and the allosteric and catalytic sites of SOS. It is possible that the combination of G13E and G75D substitutions results in an activated Ras protein that is capable of constitutive signaling but is spatially dysregulated within cells by virtue of an impaired ability to bind SOS. In this scenario, *Ras/let-60(G13E G75D)* may retain sufficient function in contexts where SOS-dependent subcellular localization of Ras activity is not critical but fail to function in contexts where the ability to bind SOS is essential. While the underlying biochemical mechanism is speculative, the phenotypes observed in *Ras/let-60(G13E G75D)* animals reveal a novel genetic interaction by which an activating mutation interacts with a putative loss of function substitution in the switch II region of *Ras/let-60* to differentially affect downstream responses.

Unexpectedly, cell type-specific depletion of key cytoskeletal regulators including homologs of Rac, RhoG, ARP2, WAVE, WASP, and ROCK did not severely affect SM migration, although we observed a spectrum of other defects in M lineage development. Taken together, these results indicate considerable redundancy among cytoskeletal regulatory proteins during cell migration *in vivo*. Developmental roles for essential cytoskeletal regulators are challenging to dissect in living animals due to lethality or pleiotropic effects, and our understanding of how these proteins function in cell migration comes largely from experiments in cell culture or in mutants, with associated caveats[61,81]. While our results were unexpected given the prominence of dynamic, branched actin networks in crawling cell motility, the Arp2/3 complex has also been shown to be dispensable for cultured fibroblast chemotaxis in response to a PDGF gradient[71]. Here, we used timed, cell type-specific depletion of endogenous proteins to circumvent pleiotropic effects and found no major roles in SM migration. While we cannot definitively rule out the possibility of incomplete protein depletion in SMs, the presence of cell division defects in the M-lineage and lethality caused by ubiquitous depletion suggests that these tools are capable of ablating protein function. With some promoters, TIR1 levels can be limiting for degrading AID-tagged proteins. However, out of the endogenous proteins that we targeted in SMs, we observed strong depletion phenotypes for the three genes with highest expression in SMs based on L2 scRNAseq data[44] (*egl-15*, *let-60*, and *sos-1*; Figure S9), indicating that TIR1 was expressed at levels sufficient for effective depletion in migrating SMs. Future experiments to test roles for additional cytoskeletal regulators and/or combinations will be important to complete our understanding of how an extracellular FGF signal is translated into the cytoskeletal remodeling and force generation required for directed cell migration in SMs. Our results suggesting that

SOS-1 instructs SM orientation while activated Ras/LET-60 acts permissively raise the question of what effectors act downstream of SOS-1 to execute its instructive role. Although SOS proteins can directly activate Rac in some contexts[8], *Rac/ced-10* mutants do not have defects in SM migration, and we observed only minor effects on SM migration after simultaneously depleting Rac/CED-10 and RhoG/MIG-2. Identifying additional proteins that interact with SOS-1 during RTK-mediated migration will also be crucial for deepening our understanding of directional cell movement.

An endogenously tagged protein toolkit to dissect RTK signaling and cell dynamics *in vivo*

Our systematic approach to depleting endogenous signal transduction and regulatory proteins in specific cell types was a critical factor in dissecting how an RTK regulates cell migration in a living animal. In doing so, we have generated a toolkit of 16 endogenously tagged proteins that provide new and valuable tools to elucidate cellular and developmental mechanisms *in vivo* with spatial and temporal precision. These include key proteins involved in SOS, Ras, ERK, PI3K, Akt, and mTOR signaling along with cytoskeletal regulators important for many aspects of cell physiology and cellular behavior[4,69,82,83]. Notably, this toolkit includes functional mScarlet-I and AID-tagged alleles for Ras/LET-60, which is a protein of intense interest due to its biomedical significance that has been recalcitrant to endogenous tagging without disrupting its function[42]. Because RTK signaling and cytoskeletal remodeling have critical roles in many developmental and homeostatic processes[5,61,72], the endogenously tagged proteins generated in this study provide a powerful toolkit for researchers exploring a wide range of biological questions. For example, the discovery that cell type-specific depletion of mTOR/LET-363 leads to miniscule M lineage cells provides insights into cell size control, and the ability to control mTOR/LET-363 levels in space and time will be valuable to researchers investigating autophagy and aging[49]. These tools have already provided an unprecedented, high-resolution view of how cells migrate towards a directional cue in *C. elegans*. Together, our findings shed light on how RTK signaling drives directed cell migration in living animals and highlight the diversity of signal transduction and cell migratory mechanisms that mediate animal development.

Acknowledgements

pWZ234 was a gift of David Matus. We also thank Min Han for supporting the genetic screen that originally identified *let-60(n1046ku75)* and Arun Dutta for their feedback on the manuscript. Some strains were provided by the CGC, which is funded by the NIH Office of Research Infrastructure Programs (P40 OD010440). This work was funded by National Institutes of Health grants R35GM142880 (AMP), R35GM136315 (MVS) and R35GM144237 (DJR) and predoctoral fellowship F31HD112152 (TVG).

Author Contributions

Conceptualization, TVG, AMP; methodology, TVG., JIM, NRR, LL, DJR, MVS, AMP; formal analysis, TVG; investigation, TVG, MVS, AMP; data curation. TVG, AMP; writing – original draft, TVG; writing – review & editing, TVG, MVS, DJR, AMP; visualization, TVG and AMP; project administration, AMP; funding acquisition, TVG, MVS, DJR, AMP.

Resource availability

Lead contact

For further inquiries or requests for obtaining reagents and resources generated in this study, please contact. Ariel Pani at amp2na@virginia.edu.

Materials availability

C. elegans strains generated in this study will be deposited at the CGC (https://cgc.umn.edu/) upon manuscript acceptance. Plasmids and other reagents will be shared on request.

Data and code availability

Source data used to analyze SM positioning for all strains are summarized in Table 1. Original confocal images and raw migration data are available upon request. No code was generated in this study.

Declaration of Interests

The authors declare no competing interests.

Materials and Methods

C. elegans maintenance

C. elegans strains generated in this study were originally derived from the N2 Bristol strain (wild-type) and are listed in the Resources and Reagents table. Worms were maintained and experiments were performed at room temperature (22°C). Standard *C. elegans* culturing conditions were followed[84], with animals grown on Nematode Growth Medium (NGM) plates seeded with *Escherichia coli* OP50[84].

Plasmid construction

Repair templates for genome engineering were cloned constructed using Gibson assembly and Cas9 + sgRNA plasmids were cloned using site-directed mutagenesis as described previously[85]. Sequences used for repair template design were downloaded from Wormbase[86]. Primers and double stranded synthetic DNA fragments (gBlocks) were ordered from Integrated DNA Technologies (IDT). Constructs were transformed into chemically competent *E. coli* 5-alpha cells (NEB C2987). Plasmid DNA was extracted using either Qiagen (Qiagen 27104) or Invitrogen PureLink HQ (Invitrogen K210010) miniprep kits. Plasmids were verified by Sanger sequencing (GENEWIZ) and/or whole-plasmid nanopore sequencing (Plasmidsaurus) before use. To generate the sem-5::PH(internal)::mNG construct (pTG421), the internal SH2 domain (amino acids ITRNDAEVLLKKPTVRDGHLVRQCESSPGEFSISVRFQDSVQHFK) was replaced with a PH domain from *Rattus norvegicus plc1δ1* that is common used for plasma membrane localization of fluorescent proteins in *C. elegans*[87]. To enhance expression efficiency, the DNA sequences coding for *egl-17*, the SOS catalytic domain[57], and *let-60(G13E)* were codon-optimized using the *C. elegans* codon adapter tool[88] (https://worm.mpi-cbg.de/codons/cgi-bin/optimize.py). We used a germline codon optimized[89] sequence for the *mScarlet-I::let-60* knock-in. A comprehensive list of all plasmids generated or used in this study, including the appropriate plasmid backbones and vectors used for cloning, is provided in Resources and Reagents. Promoter sequences used are provided in Supplemental File 1.

C. elegans genome engineering and transgenesis

Fluorescent protein::AID knock-in strains were generated using Cas9-triggered homologous recombination with a self-excising selection cassette[85]. Injections were performed with a paintbrush to increase survival as previously described[90]. Fluorescent protein insertion sites were selected based on protein domain function and structure where possible. Guide RNA target sites were selected based on proximity to the desired insertion site and predicted off-target sites using ChopChop[91] (https://chopchop.cbu.uib.no/). When the guide sequence was present in the repair template itself, we introduced synonymous mutations to prevent cleavage of the repair template by Cas9. Guide sequences and insertion sites are detailed in Supplemental File 1. Due to the compact structure of Ras/LET-60, we found it was necessary to use a 30 amino acid flexible linker to generate biologically functional knock-in alleles. Due to low efficiency of the guide RNA targeting the *Ras/let-60* N-terminus, we inserted a known, high-efficiency gRNA site derived from *dpy-10* at the N-terminus of endogenous *Ras/let-60* using co-CRISPR to generate *let-60(re302[d10::let-60])*. This allele was viable as a homozygote and confirmed by sequencing. We then used this efficient guide RNA site within *let-60(re302)* to engineer N-terminal *Ras/let-60* knock-ins using co-CRISPR with a *dpy-10* guide RNA. We were unable to recover homozygous mScarlet-I::AID::Ras/LET-60 knock-in animals, suggesting this fusion was not functional. However, we were able to separately generate functional mScarlet-I::Ras/LET-60 and AID::Ras/LET-60 alleles that allowed for visualization and depletion of the endogenous protein in complementary strains. Microinjection mixes for PCR fragment-based knock-ins were templates were prepared as previously described[92], and crRNA and ssODN sequences are provided in Reagents and Resources table and Supplemental File 1. The PI3K/AGE-1::mNG::AID knock-in allele was generated by inserting mNG::AID before the WIF (Wortmannin-Insensitive Fragment) motif to preserve protein function (see Supplemental File 1). Because the SEC truncated *age-1* in the initial insertion strain, we heat-shocked heterozygous *age-1::mNG^SEC^AID* animals to excise the SEC and isolated heterozygous *age-1::mNG::AID/WT* animals by picking fluorescent animals with wild-type movement under a fluorescence microscope. APL127 was then derived from homozygous self-progeny of a heterozygous SEC-excised animal. APL306 was constructed by crossing APL127 and APL173. The SEC could not be excised from the *Phlh-8>sem-5::PH::mNG SEC* transgene in the parent strain of APL481 despite repeated heat shock attempts. To accurately score SM positioning in this strain, we eliminated the rolling phenotype caused by the SEC by knocking out the synthetic *sqt-1(d)* allele using a crRNA specific to the codon-optimized *sqt-1* sequence used in the SEC and a single stranded oligonucleotide repair template (Supplemental File 1). SpCas9 protein and TracrRNA were then co-injected, following the standard Co-CRISPR protocol[93], and non-rolling worms were selected in the next generation. All endogenously tagged strains used in this study appeared superficially wild-type, with the exception of APL496 (*mNG::AID::RhoG/mig-2* + *mScarlet-I::AID::Rac/ced-10*). While the SMs consistently migrated correctly in this strain, we occasionally observed abnormal SM divisions after migration. Additionally, adult worms sometimes exhibited germline defects and protruding vulvas, indicating that this combination of tags causes partial loss of function. A comprehensive list of all strains, endogenous protein tags, linker sequences, guide RNA targets, and specific insertion locations can be found in the Reagents and Resources table and/or Supplemental File 1.

Strains APL430, APL499, and APL885 were generated using co-CRISPR with single-stranded oligodeoxynucleotide repair templates. Repair templates and guide RNAs were designed following established protocols[93]. SpCas9 protein, single stranded DNA repair templates, tracrRNA, and crRNAs were ordered from Integrated DNA Technologies. Sequences are available in Supplemental File 1. The *FGFR/egl-15(ljf54)* mutant was isolated by screening for egg-laying deficient animals in the F2 generation. The *Ras/let-60(G13E)* mutant *let-60(ljf52)* was isolated by screening for the semidominant multivulval phenotype caused by Ras/LET-60 gain of function. The *Ras/let-60(G13E G75D)* allele *let-60(ljf53)* was generated by co-CRISPR in the *let-60(ljf52)* background. *let-60(ljf53)* was isolated by screening for F2 animals where the multivulval phenotype was suppressed. Oligonucleotide repair template and crRNA sequences are provided in Supplemental File 1. Genomic edits were sequence-verified by sequencing PCR products amplified from genomic DNA of homozygous animals. All transgenic strains were generated by single copy insertions at safe harbor sites using Cas9-triggered homologous recombination with the SEC approach[85]. Transgenes were inserted near the ttTi4348 site on Chr I[94] or a site used for efficient single copy insertions on ChrIV[31]. Guide RNA and homology arm sequences used for transgenes are provided in Supplemental File 1.

Endogenously tagged protein depletion with K-NAA

AID-tagged proteins were depleted by treating with the water soluble, synthetic auxin 1-Naphthaleneacetic Acid Potassium Salt (K-NAA)[37]. To deplete AID-tagged proteins, we treated entire plates of worms by adding 400 µL of a 100 mM K-NAA solution for a final concentration of 4 mM per plate. Plates were then allowed to dry with the lid ajar. The K-NAA stock solution was prepared in nuclease free water, stored at 4°C, and replaced every 3-4 weeks. Paired control plates were treated with nuclease free water. For timed depletion experiments, we used bleach synchronization[84] to produce plates of synchronized L1 stage animals. Prior to K-NAA treatment, we confirmed developmental staging in a subsample of animals on each plate using spinning disk confocal microscopy. Staging was determined based on external anatomy, vulval morphology, and M lineage development to ensure consistency[95]. Once developmental stages were verified, K-NAA was immediately added to the plates.

We took several approaches to validate depletion phenotypes for target proteins whose depletion did not result in M lineage defects. To confirm that our AID-tagged alleles were capable of ablating protein function, we also used whole-body depletion with a ubiquitously expressed TIR1 transgene. For all strains described here, ubiquitous depletion phenocopied the known null mutant phenotypes, indicating these alleles are capable of eliminating the essential functions of the targeted proteins. For genes with viable null mutations, we examined M lineage phenotypes and SM migration in null mutants (*age-1(m333), ksr-1(n2526), abl-1(ok171)*).

Identification of *let-60(n1046ku75)*

The *let-60(n1046ku75)* mutant was isolated in a mutagenesis screen to identify factors acting downstream of Ras/LET-60 in vulval development. Briefly, *let-60(n1046gf)* hermaphrodites were mutagenized with 50 mM ethyl methanesulfonate (EMS) and allowed to self-fertilize for two generations. F2 grand progeny were screened for non-multivulval animals to identify suppressors of activated Ras/LET-60. Candidate suppressor strains were backcrossed to the

parent *let-60(n1046gf)* strain, and mutations were placed on a genetic map using phenotypic mapping strains as described previously[96,97]. To identify the molecular lesion responsible for *ku75, let-60* coding sequences were PCR amplified from the parental *let-60(n1046gf)* strain and *ku75* and directly sequenced (Figure S6).

Microscopy and Image Processing

For live imaging, multiple worms from the same strain or experimental manipulation were anesthetized in a drop (~4 µL) of 0.2 mM levamisole in M9 buffer on a 170 ± 5 µm glass coverslip and allowed to rest for several minutes before being mounted on 2-5% agarose pads[98]. Worms were imaged or scored for SM positioning within 1 hour of mounting. All images were acquired by live imaging using either a Yokogawa CSU-X1 spinning disk confocal equipped with a Hamamatsu ORCA Fusion BT CMOS camera, or a Yokogawa CSU-W1 SoRA spinning disk confocal equipped with a Hamamatsu ORCA Quest qCMOS camera. Both imaging systems were mounted on Nikon Ti2 inverted microscope stands with perfect focus. Imaging was performed using excitation lasers at 445 nm, 514 nm, 561 nm, or 594 nm depending on the fluorescent protein. For the CSU-W1 SoRA system, imaging was performed with either a Nikon SR Plan Apo IR 60X/1.27 water immersion objective or a Nikon Apo TIRF 100X/1.49 oil immersion objective. The CSU-X1 system utilized a Nikon Apo TIRF 100X/1.49 oil objective, a Nikon Apo TIRF 60X/1.49 oil objective, or a Nikon S Fluor 40X/1.30 oil objective. Images were acquired using Nikon NIS-Elements software (Versions AR 5.42.06 and AR 5.42.04) with z-step sizes, camera exposure times, and laser intensities adjusted based on fluorescence intensities of the tagged proteins. Images of endogenously tagged proteins were deconvolved, and images of plasma membrane markers were denoised, using Nikon NIS Elements software. For figure preparation, we adjusted brightness and contrast using Fiji[99]. Animals in Figures 1C and 4E were computationally straightened in Fiji to more clearly compare SM positions.

Cell position scoring and statistical analyses

To compare SM migration between strains, we scored SM positioning at the developmental stage when SMs have normally completed their migration but just prior to their initial division. To ensure accurate scoring in animals with SM migration failures, we used VPC, gonad, and body wall muscle development to establish developmental timing. SM positions were scored based on established landmarks including the positions of the vulval precursor cells and M lineage-derived body wall muscles that are visible using the same transgene used to visualize SM positions (Figure S1A). Positions of these cells were unaffected in all auxin-treated strains. The SM position was scored based on the visual center of each cell (two SMs per animal), and scored on a scale from 0 (representing a cell centered correctly over P6.p) to 7 (the most posterior position observed) to reflect the range of migration phenotypes observed. Any position other than 0 represents a migration defect. At least 30 animals (60 SMs) were included for each experimental condition with no data points excluded from analysis post-hoc. Statistical analyses to compare frequency distributions of SM positions were conducted using Fisher's exact test (two-tailed) calculated in Microsoft Excel (Version 16.89.1). P-values were considered significant at $P<0.05$. For manipulations that affected dorsoventral SM positioning, we used a

standard contingency table and chi-squared test to compare the percentages of dorsoventral defects between strains.

References

1. Sherwood, D.R., and Plastino, J. (2018). Invading, leading and navigating cells in Caenorhabditis elegans: Insights into cell movement in vivo. Genetics *208*, 53–78.

2. SenGupta, S., Parent, C.A., and Bear, J.E. (2021). The principles of directed cell migration. Nat. Rev. Mol. Cell Biol. *22*, 529–547.

3. Dormann, D., and Weijer, C.J. (2003). Chemotactic cell movement during development. Curr. Opin. Genet. Dev. *13*, 358–364.

4. Devreotes, P., and Horwitz, A.R. (2015). Signaling networks that regulate cell migration. Cold Spring Harb. Perspect. Biol. *7*, a005959.

5. Lemmon, M.A., and Schlessinger, J. (2010). Cell signaling by receptor tyrosine kinases. Cell *141*, 1117–1134.

6. Casaletto, J.B., and McClatchey, A.I. (2012). Spatial regulation of receptor tyrosine kinases in development and cancer. Nat. Rev. Cancer *12*, 387–400.

7. Simanshu, D.K., Nissley, D.V., and McCormick, F. (2017). RAS proteins and their regulators in human disease. Cell *170*, 17–33.

8. Innocenti, M., Tenca, P., Frittoli, E., Faretta, M., Tocchetti, A., Di Fiore, P.P., and Scita, G. (2002). Mechanisms through which Sos-1 coordinates the activation of Ras and Rac. J. Cell Biol. *156*, 125–136.

9. Cuesta, C., Arévalo-Alameda, C., and Castellano, E. (2021). The importance of being PI3K in the RAS signaling network. Genes (Basel) *12*, 1094.

10. Sundaram, M.V. Canonical RTK-Ras-ERK signaling and related alternative pathways. http://www.wormbook.org/chapters/www_RTKRasMAPKsignaling.2/RTKRasERKsignal.html.

11. Balasubramanian, R., and Zhang, X. (2016). Mechanisms of FGF gradient formation during embryogenesis. Semin. Cell Dev. Biol. *53*, 94–100.

12. Sato, M., and Kornberg, T.B. (2002). FGF is an essential mitogen and chemoattractant for the air sacs of the drosophila tracheal system. Dev. Cell *3*, 195–207.

13. Toyoda, R., Assimacopoulos, S., Wilcoxon, J., Taylor, A., Feldman, P., Suzuki-Hirano, A., Shimogori, T., and Grove, E.A. (2010). FGF8 acts as a classic diffusible morphogen to pattern the neocortex. Development *137*, 3439–3448.

14. Song, Y.H., Zhu, Y.T., Ding, J., Zhou, F.Y., Xue, J.X., Jung, J.H., Li, Z.J., and Gao, W.Y. (2016). Distribution of fibroblast growth factors and their roles in skin fibroblast cell migration. Mol. Med. Rep. *14*, 3336–3342.

15. Maretzky, T., Evers, A., Zhou, W., Swendeman, S.L., Wong, P.-M., Rafii, S., Reiss, K., and Blobel, C.P. (2011). Migration of growth factor-stimulated epithelial and endothelial cells depends on EGFR transactivation by ADAM17. Nat. Commun. *2*, 229.

16. Guzzetta, A., Koska, M., Rowton, M., Sullivan, K.R., Jacobs-Li, J., Kweon, J., Hidalgo, H., Eckart, H., Hoffmann, A.D., Back, R., et al. (2020). Hedgehog-FGF signaling axis patterns anterior mesoderm during gastrulation. Proc. Natl. Acad. Sci. U. S. A. *117*, 15712–15723.

17. Sutherland, D., Samakovlis, C., and Krasnow, M.A. (1996). branchless encodes a Drosophila FGF homolog that controls tracheal cell migration and the pattern of branching. Cell *87*, 1091–1101.

18. Li, S., and Muneoka, K. (1999). Cell migration and chick limb development: chemotactic action of FGF-4 and the AER. Dev. Biol. *211*, 335–347.

19. Yang, X., Dormann, D., Münsterberg, A.E., and Weijer, C.J. (2002). Cell movement patterns during gastrulation in the chick are controlled by positive and negative chemotaxis mediated by FGF4 and FGF8. Dev. Cell *3*, 425–437.

20. Roussigné, M., Wei, L., Tsingos, E., Kuchling, F., Alkobtawi, M., Tsalavouta, M., Wittbrodt, J., Carl, M., Blader, P., and Wilson, S.W. (2018). Left/right asymmetric collective migration of parapineal cells is mediated by focal FGF signaling activity in leading cells. Proc. Natl. Acad. Sci. U. S. A. *115*, E9812–E9821.

21. Yamada, K.M., and Sixt, M. (2019). Mechanisms of 3D cell migration. Nat. Rev. Mol. Cell Biol. *20*, 738–752.

22. Kuhn, J., Lin, Y., and Devreotes, P.N. (2021). Using Live-Cell Imaging and Synthetic Biology to Probe Directed Migration in Dictyostelium. Front Cell Dev Biol *9*, 740205.

23. Pudewell, S., Wittich, C., Kazemein Jasemi, N.S., Bazgir, F., and Ahmadian, M.R. (2021). Accessory proteins of the RAS-MAPK pathway: moving from the side line to the front line. Commun. Biol. *4*, 696.

24. Chioni, A.-M., and Grose, R. (2012). FGFR1 cleavage and nuclear translocation regulates breast cancer cell behavior. J. Cell Biol. *197*, 801–817.

25. Samson, S.C., Khan, A.M., and Mendoza, M.C. (2022). ERK signaling for cell migration and invasion. Front. Mol. Biosci. *9*, 998475.

26. Hirashima, T., Hino, N., Aoki, K., and Matsuda, M. (2023). Stretching the limits of extracellular signal-related kinase (ERK) signaling - Cell mechanosensing to ERK activation. Curr. Opin. Cell Biol. *84*, 102217.

27. Branda, C.S., and Stern, M.J. (2000). Mechanisms controlling sex myoblast migration in Caenorhabditis elegans hermaphrodites. Dev. Biol. *226*, 137–151.

28. Sulston, J.E., and Horvitz, H.R. (1977). Post-embryonic cell lineages of the nematode, Caenorhabditis elegans. Dev. Biol. *56*, 110–156.

29. Burdine, R.D., Branda, C.S., and Stern, M.J. (1998). EGL-17(FGF) expression coordinates

the attraction of the migrating sex myoblasts with vulval induction in C. elegans. Development *125*, 1083–1093.

30. Burdine, R.D., Chen, E.B., Kwok, S.F., and Stern, M.J. (1997). egl-17 encodes an invertebrate fibroblast growth factor family member required specifically for sex myoblast migration in Caenorhabditis elegans. Proc. Natl. Acad. Sci. U. S. A. *94*, 2433–2437.

31. Gibney, T.V., and Pani, A.M. (2025). FGF diffusion is required for directed migration of postembryonic muscle progenitors in C. elegans. bioRxiv, 2025.03.19.643693. https://doi.org/10.1101/2025.03.19.643693.

32. Stern, M.J., and Horvitz, H.R. (1991). A normally attractive cell interaction is repulsive in two C. elegans mesodermal cell migration mutants. Development *113*, 797–803.

33. Sundaram, M., Yochem, J., and Han, M. (1996). A Ras-mediated signal transduction pathway is involved in the control of sex myoblast migration in Caenorhabditis elegans. Development *122*, 2823–2833.

34. O'Keeffe, C., and Greenwald, I. (2022). EGFR signal transduction is downregulated in C. elegans vulval precursor cells during dauer diapause. Development *149*, dev201094.

35. Beitel, G.J., Clark, S.G., and Horvitz, H.R. (1990). Caenorhabditis elegans ras gene let-60 acts as a switch in the pathway of vulval induction. Nature *348*, 503–509.

36. Han, M., and Sternberg, P.W. (1990). let-60, a gene that specifies cell fates during C. elegans vulval induction, encodes a ras protein. Cell *63*, 921–931.

37. Martinez, M.A.Q., and Matus, D.Q. (2020). Auxin-mediated protein degradation in Caenorhabditis elegans. Bio Protoc. *10*. https://doi.org/10.21769/BioProtoc.3589.

38. Zhang, L., Ward, J.D., Cheng, Z., and Dernburg, A.F. (2015). The auxin-inducible degradation (AID) system enables versatile conditional protein depletion in C. elegans. Development *142*, 4374–4384.

39. Harfe, B.D., Vaz Gomes, A., Kenyon, C., Liu, J., Krause, M., and Fire, A. (1998). Analysis of a Caenorhabditis elegans Twist homolog identifies conserved and divergent aspects of mesodermal patterning. Genes Dev. *12*, 2623–2635.

40. Meyers, S.G., and Corsi, A.K. (2010). C. elegans twist gene expression in differentiated cell types is controlled by autoregulation through intron elements. Dev. Biol. *346*, 224–236.

41. Goodman, S.J., Branda, C.S., Robinson, M.K., Burdine, R.D., and Stern, M.J. (2003). Alternative splicing affecting a novel domain in the C. elegans EGL-15 FGF receptor confers functional specificity. Development *130*, 3757–3766.

42. Jayadev, R., Chi, Q., and Sherwood, D.R. (2023). Post-embryonic endogenous expression and localization of LET-60/Ras in C. elegans. MicroPubl. Biol. *2023*, 10.17912/micropub.biology.000931.

43. DeVore, D.L., Horvitz, H.R., and Stern, M.J. (1995). An FGF receptor signaling pathway is required for the normal cell migrations of the sex myoblasts in C. elegans hermaphrodites.

Cell *83*, 611–620.

44. Ben-David, E., Boocock, J., Guo, L., Zdraljevic, S., Bloom, J.S., and Kruglyak, L. (2021). Whole-organism eQTL mapping at cellular resolution with single-cell sequencing. Elife *10*. https://doi.org/10.7554/eLife.65857.

45. Church, D.L., Guan, K.L., and Lambie, E.J. (1995). Three genes of the MAP kinase cascade, mek-2, mpk-1/sur-1 and let-60 ras, are required for meiotic cell cycle progression in Caenorhabditis elegans. Development *121*, 2525–2535.

46. Lackner, M.R., Kornfeld, K., Miller, L.M., Horvitz, H.R., and Kim, S.K. (1994). A MAP kinase homolog, mpk-1, is involved in ras-mediated induction of vulval cell fates in Caenorhabditis elegans. Genes Dev. *8*, 160–173.

47. Paradis, S., and Ruvkun, G. (1998). Caenorhabditis elegans Akt/PKB transduces insulin receptor-like signals from AGE-1 PI3 kinase to the DAF-16 transcription factor. Genes Dev. *12*, 2488–2498.

48. Morris, J.Z., Tissenbaum, H.A., and Ruvkun, G. (1996). A phosphatidylinositol-3-OH kinase family member regulating longevity and diapause in Caenorhabditis elegans. Nature *382*, 536–539.

49. Blenis, J. (2017). TOR, the gateway to cellular metabolism, cell growth, and disease. Cell *171*, 10–13.

50. Dorey, K., and Amaya, E. (2010). FGF signalling: diverse roles during early vertebrate embryogenesis. Development *137*, 3731–3742.

51. Sivak, J.M., Petersen, L.F., and Amaya, E. (2005). FGF signal interpretation is directed by Sprouty and Spred proteins during mesoderm formation. Dev. Cell *8*, 689–701.

52. Nutt, S.L., Dingwell, K.S., Holt, C.E., and Amaya, E. (2001). Xenopus Sprouty2 inhibits FGF-mediated gastrulation movements but does not affect mesoderm induction and patterning. Genes Dev. *15*, 1152–1166.

53. Yin, X., Gower, N.J.D., Baylis, H.A., and Strange, K. (2004). Inositol 1,4,5-trisphosphate signaling regulates rhythmic contractile activity of myoepithelial sheath cells in Caenorhabditis elegans. Mol. Biol. Cell *15*, 3938–3949.

54. Van Buskirk, C., and Sternberg, P.W. (2007). Epidermal growth factor signaling induces behavioral quiescence in Caenorhabditis elegans. Nat. Neurosci. *10*, 1300–1307.

55. McKay, M.M., and Morrison, D.K. (2007). Integrating signals from RTKs to ERK/MAPK. Oncogene *26*, 3113–3121.

56. Cox, A.D., Fesik, S.W., Kimmelman, A.C., Luo, J., and Der, C.J. (2014). Drugging the undruggable RAS: Mission possible? Nat. Rev. Drug Discov. *13*, 828–851.

57. Toettcher, J.E., Weiner, O.D., and Lim, W.A. (2013). Using optogenetics to interrogate the dynamic control of signal transmission by the Ras/Erk module. Cell *155*, 1422–1434.

58. Garcia, P., Gupta, R., Shah, S., Morris, A.J., Rudge, S.A., Scarlata, S., Petrova, V., McLaughlin, S., and Rebecchi, M.J. (1995). The pleckstrin homology domain of phospholipase C-delta 1 binds with high affinity to phosphatidylinositol 4,5-bisphosphate in bilayer membranes. Biochemistry *34*, 16228–16234.

59. Edwards, K.A., Demsky, M., Montague, R.A., Weymouth, N., and Kiehart, D.P. (1997). GFP-moesin illuminates actin cytoskeleton dynamics in living tissue and demonstrates cell shape changes during morphogenesis in Drosophila. Dev. Biol. *191*, 103–117.

60. Chung, W.-L., Eibauer, M., Li, W., Boujemaa-Paterski, R., Geiger, B., and Medalia, O. (2022). A network of mixed actin polarity in the leading edge of spreading cells. Commun. Biol. *5*, 1338.

61. Pollard, T.D., and Borisy, G.G. (2003). Cellular motility driven by assembly and disassembly of actin filaments. Cell *112*, 453–465.

62. Lawson, C.D., and Ridley, A.J. (2018). Rho GTPase signaling complexes in cell migration and invasion. J. Cell Biol. *217*, 447–457.

63. Lundquist, E.A., Reddien, P.W., Hartwieg, E., Horvitz, H.R., and Bargmann, C.I. (2001). Three C. elegans Rac proteins and several alternative Rac regulators control axon guidance, cell migration and apoptotic cell phagocytosis. Development *128*, 4475–4488.

64. Goetsch, K.P., Snyman, C., Myburgh, K.H., and Niesler, C.U. (2014). ROCK-2 is associated with focal adhesion maturation during myoblast migration: ROCK controls directional myoblast migration. J. Cell. Biochem. *115*, 1299–1307.

65. Sini, P., Cannas, A., Koleske, A.J., Di Fiore, P.P., and Scita, G. (2004). Abl-dependent tyrosine phosphorylation of Sos-1 mediates growth-factor-induced Rac activation. Nat. Cell Biol. *6*, 268–274.

66. Gerboth, S., Frittoli, E., Palamidessi, A., Baltanas, F.C., Salek, M., Rappsilber, J., Giuliani, C., Troglio, F., Rolland, Y., Pruneri, G., et al. (2018). Phosphorylation of SOS1 on tyrosine 1196 promotes its RAC GEF activity and contributes to BCR-ABL leukemogenesis. Leukemia *32*, 820–827.

67. Park, K.C., Rivero, F., Meili, R., Lee, S., Apone, F., and Firtel, R.A. (2004). Rac regulation of chemotaxis and morphogenesis in Dictyostelium. EMBO J. *23*, 4177–4189.

68. Faix, J., and Weber, I. (2013). A dual role model for active Rac1 in cell migration. Small GTPases *4*, 110–115.

69. Wozniak, M.A., Kwong, L., Chodniewicz, D., Klemke, R.L., and Keely, P.J. (2005). R-Ras controls membrane protrusion and cell migration through the spatial regulation of Rac and Rho. Mol. Biol. Cell *16*, 84–96.

70. Kishore, R.S., and Sundaram, M.V. (2002). ced-10 Rac and mig-2 function redundantly and act with unc-73 trio to control the orientation of vulval cell divisions and migrations in Caenorhabditis elegans. Dev. Biol. *241*, 339–348.

71. Wu, C., Asokan, S.B., Berginski, M.E., Haynes, E.M., Sharpless, N.E., Griffith, J.D.,

Gomez, S.M., and Bear, J.E. (2012). Arp2/3 is critical for lamellipodia and response to extracellular matrix cues but is dispensable for chemotaxis. Cell *148*, 973–987.

72. Neben, C.L., Lo, M., Jura, N., and Klein, O.D. (2019). Feedback regulation of RTK signaling in development. Dev. Biol. *447*, 71–89.

73. Hubbard, S.R., and Miller, W.T. (2007). Receptor tyrosine kinases: mechanisms of activation and signaling. Curr. Opin. Cell Biol. *19*, 117–123.

74. Boilly, B., Vercoutter-Edouart, A.S., Hondermarck, H., Nurcombe, V., and Le Bourhis, X. (2000). FGF signals for cell proliferation and migration through different pathways. Cytokine Growth Factor Rev. *11*, 295–302.

75. Baltanás, F.C., Zarich, N., Rojas-Cabañeros, J.M., and Santos, E. (2020). SOS GEFs in health and disease. Biochim. Biophys. Acta Rev. Cancer *1874*, 188445.

76. Rauen, K.A. (2013). The RASopathies. Annu. Rev. Genomics Hum. Genet. *14*, 355–369.

77. Pylayeva-Gupta, Y., Grabocka, E., and Bar-Sagi, D. (2011). RAS oncogenes: weaving a tumorigenic web. Nat. Rev. Cancer *11*, 761–774.

78. Bandaru, P., Shah, N.H., Bhattacharyya, M., Barton, J.P., Kondo, Y., Cofsky, J.C., Gee, C.L., Chakraborty, A.K., Kortemme, T., Ranganathan, R., et al. (2017). Deconstruction of the Ras switching cycle through saturation mutagenesis. Elife *6*, e27810.

79. Hall, B.E., Yang, S.S., Boriack-Sjodin, P.A., Kuriyan, J., and Bar-Sagi, D. (2001). Structure-based mutagenesis reveals distinct functions for Ras switch 1 and switch 2 in Sos-catalyzed guanine nucleotide exchange. J. Biol. Chem. *276*, 27629–27637.

80. Margarit, S.M., Sondermann, H., Hall, B.E., Nagar, B., Hoelz, A., Pirruccello, M., Bar-Sagi, D., and Kuriyan, J. (2003). Structural evidence for feedback activation by Ras.GTP of the Ras-specific nucleotide exchange factor SOS. Cell *112*, 685–695.

81. Swaney, K.F., and Li, R. (2016). Function and regulation of the Arp2/3 complex during cell migration in diverse environments. Curr. Opin. Cell Biol. *42*, 63–72.

82. Campa, C.C., Ciraolo, E., Ghigo, A., Germena, G., and Hirsch, E. (2015). Crossroads of PI3K and Rac pathways. Small GTPases *6*, 71–80.

83. Castellano, E., Molina-Arcas, M., Krygowska, A.A., East, P., Warne, P., Nicol, A., and Downward, J. (2016). RAS signalling through PI3-Kinase controls cell migration via modulation of Reelin expression. Nat. Commun. *7*, 11245.

84. §, T.S. Maintenance of C. elegans. http://www.wormbook.org/chapters/www_strainmaintain/strainmaintain.html.

85. Dickinson, D.J., Pani, A.M., Heppert, J.K., Higgins, C.D., and Goldstein, B. (2015). Streamlined genome engineering with a self-excising drug selection cassette. Genetics *200*, 1035–1049.

86. Sternberg, P.W., Van Auken, K., Wang, Q., Wright, A., Yook, K., Zarowiecki, M., Arnaboldi,

V., Becerra, A., Brown, S., Cain, S., et al. (2024). WormBase 2024: status and transitioning to Alliance infrastructure. Genetics *227*, iyae050.

87. Heppert, J.K., Dickinson, D.J., Pani, A.M., Higgins, C.D., Steward, A., Ahringer, J., Kuhn, J.R., and Goldstein, B. (2016). Comparative assessment of fluorescent proteins for in vivo imaging in an animal model system. Mol. Biol. Cell *27*, 3385–3394.

88. Redemann, S., Schloissnig, S., Ernst, S., Pozniakowsky, A., Ayloo, S., Hyman, A.A., and Bringmann, H. (2011). Codon adaptation-based control of protein expression in C. elegans. Nat. Methods *8*, 250–252.

89. Fielmich, L.-E., Schmidt, R., Dickinson, D.J., Goldstein, B., Akhmanova, A., and van den Heuvel, S. (2018). Optogenetic dissection of mitotic spindle positioning in vivo. Elife *7*. https://doi.org/10.7554/eLife.38198.

90. Gibney, T.V., Favichia, M., Latifi, L., Medwig-Kinney, T.N., Matus, D.Q., McIntyre, D.C., Arrigo, A.B., Branham, K.R., Bubrig, L.T., Ghaddar, A., et al. (2023). A simple method to dramatically increase C. elegans germline microinjection efficiency. Dev. Biol. *502*, 63–67.

91. Labun, K., Montague, T.G., Krause, M., Torres Cleuren, Y.N., Tjeldnes, H., and Valen, E. (2019). CHOPCHOP v3: expanding the CRISPR web toolbox beyond genome editing. Nucleic Acids Res. *47*, W171–W174.

92. Ghanta, K.S., and Mello, C.C. (2020). Melting dsDNA donor molecules greatly improves precision genome editing in Caenorhabditis elegans. Genetics *216*, 643–650.

93. Paix, A., Folkmann, A., and Seydoux, G. (2017). Precision genome editing using CRISPR-Cas9 and linear repair templates in C. elegans. Methods *121-122*, 86–93.

94. Pani, A.M., and Goldstein, B. (2018). Direct visualization of a native Wnt in vivo reveals that a long-range Wnt gradient forms by extracellular dispersal. Elife *7*. https://doi.org/10.7554/eLife.38325.

95. Sternberg, P.W. Vulval development. http://www.wormbook.org/chapters/www_vulvaldev/vulvaldev.html.

96. Sundaram, M., and Han, M. (1995). The C. elegans ksr-1 gene encodes a novel Raf-related kinase involved in Ras-mediated signal transduction. Cell *83*, 889–901.

97. Wu, Y., and Han, M. (1994). Suppression of activated Let-60 ras protein defines a role of Caenorhabditis elegans Sur-1 MAP kinase in vulval differentiation. Genes Dev. *8*, 147–159.

98. Chai, Y., Li, W., Feng, G., Yang, Y., Wang, X., and Ou, G. (2012). Live imaging of cellular dynamics during Caenorhabditis elegans postembryonic development. Nat. Protoc. *7*, 2090–2102.

99. Schindelin, J., Arganda-Carreras, I., Frise, E., Kaynig, V., Longair, M., Pietzsch, T., Preibisch, S., Rueden, C., Saalfeld, S., Schmid, B., et al. (2012). Fiji: an open-source platform for biological-image analysis. Nat. Methods *9*, 676–682.

100. Ashley, G.E., Duong, T., Levenson, M.T., Martinez, M.A.Q., Johnson, L.C., Hibshman, J.D., Saeger, H.N., Palmisano, N.J., Doonan, R., Martinez-Mendez, R., et al. (2021). An expanded auxin-inducible degron toolkit for Caenorhabditis elegans. Genetics *217*. https://doi.org/10.1093/genetics/iyab006.

101. Dickinson, D.J., Ward, J.D., Reiner, D.J., and Goldstein, B. (2013). Engineering the Caenorhabditis elegans genome using Cas9-triggered homologous recombination. Nat. Methods *10*, 1028–1034.

102. Vidal, B., Gulez, B., Cao, W.X., Leyva-Díaz, E., Reilly, M.B., Tekieli, T., and Hobert, O. (2022). The enteric nervous system of the C. elegans pharynx is specified by the Sine oculis-like homeobox gene ceh-34. Elife *11*. https://doi.org/10.7554/eLife.76003.

Figure and Video Legends

Figure 1. FGFR, GRB2, SOS, and Ras homologs are cell-autonomously required for SM migration independent of KSR or ERK. (**A**) Schematic of the TIR1-AID system for conditional protein depletion in *C. elegans.* AID-tagged proteins of interest (POI) are targeted for proteasomal degradation in the presence of TIR and auxin, or its synthetic analog K-NAA. (**B**) Representative images of SM positioning in wild-type and *FGFR/egl-15(n1458)* mutant animals. (**C**) Schematic diagram of the FGFR-GRB2-SOS-Ras-ERK signaling module. *C. elegans* homologs are indicated in parentheses. White triangles indicate the normal endpoint of migration over the P6.p cell. Dashed arrow indicates the approximate extent of migration. (**D**) Dot plot summarizing SM migration endpoints after M-lineage specific depletion of endogenously tagged proteins or in mutant strains. Area of each dot is proportional to the frequency of cells stopping at that position. Asterisks indicate statistical significance compared to wild-type animals (Fisher's exact test, *** indicates $p < 0.0005$). n>60 for all strains shown. Source data available in Table S1. (**E**) Representative, live spinning disk confocal images showing SM positioning and localization of endogenously tagged proteins in control and K-NAA-treated animals. The AID::Ras/LET-60 tag does not include a fluorescent protein. SMs are outlined in yellow in single channel images of tagged endogenous proteins, and white triangles denote the normal endpoint of SM migration. The small, circular objects visible in both fluorescence channels are autofluorescent gut granules. All images are oriented with anterior to left and dorsal to top. Scale bars = 10μm.

Figure 2. PI3K, AKT, mTOR, and PLCγ homologs are not required cell-autonomously for SM migration. (A) Schematic diagram of the conserved PI3K-Akt-mTOR signaling module along with components of the FGFR-GRB2-SOS-Ras module found to be required for SM migration. *C. elegans* homologs are indicated in parentheses. **(B)** Dot plot summarizing SM migration endpoints after M-lineage specific depletion of endogenously tagged proteins or in mutant strains. Area of each dot is proportional to the frequency of cells stopping at that position. Asterisks indicate statistical significance compared to wild-type animals (Fisher's exact test, * indicates $p<0.05$. n>60 for all strains shown. Source data available in Table S1. **(C)** Representative, live spinning disk confocal images showing SM positioning and localization of endogenously tagged proteins of interest in control and K-NAA-treated animals. SMs are outlined in yellow in single channel images of tagged endogenous proteins, and white triangles denote the normal endpoint of SM migration. The small, circular objects visible in both fluorescence channels are autofluorescent gut granules. All images are oriented with anterior to left and dorsal to top. **(D)** Representative, live spinning disk confocal image showing control vs. K-NAA-treated mNG::AID::mTOR/LET-363 animals raised with continuous K-NAA treatment. The upper two images show L3 stage animals when the SMs have completed migrating but have not started to proliferate. The lower two images show L4 stage animals at a time when the SMs have finished proliferating. (**E**) Control and K-NAA-treated mNG::AID::mTOR/LET-363 worms with timed protein depletion. K-NAA was added after the SMs are born, but several hours prior to migration, in order to circumvent early M lineage defects. Background subtraction[31] was used to remove gut granules in D and E to better visualize the abnormally small M lineage cells. All images are oriented with anterior to left and dorsal to top. Scale bars = 10μm.

Figure 3. Extracellular FGF orients SOS-1 to the leading edge of migrating SMs. (A) Representative, live spinning disk confocal images showing endogenous mNG::AID::SOS-1 localization during SM migration. **(B)** Individual frames from a time-lapse image showing mNG::AID::SOS-1 localization in a migrating SM during the early phase of FGF-dependent migration. mNG::AID::SOS-1 punctae are prominent at the front of the cell and in leading edge protrusions as the cell migrates. Images correspond to frames from Video 1. Time is in minutes:seconds. (**C)** Representative, live spinning disk confocal images showing endogenous GRB2/SEM-5::mScarlet-I::AID localization during SM migration. **(D)** Representative, live spinning disk confocal images showing endogenous mScarlet-I::Ras/LET-60 localization during SM migration. **(E)** Representative, live spinning disk confocal images showing endogenous mNG::AID::SOS-1 localization during SM migration in an *FGFR/egl-15(n1458)* mutant background. Note the absence of mNG::AID::SOS-1 punctae at the cell membrane. **(F)** Representative, live spinning disk confocal images showing mNG::AID::SOS-1 localization during SM migration in a background where FGF/EGL-17 is misexpressed near the tail to cause SMs to migrate posteriorly. mNG::AID::SOS-1 punctae localize to the posterior end of the SM as it migrates towards a posterior FGF source. Circular objects visible in both fluorescence channels are autofluorescent gut granules. An mpl-magma Look Up Table (Fiji) was used to visualize endogenously tagged protein localization in single channel images. All images are oriented with anterior to left and dorsal to top. Scale bars = 10μm.

Figure 4. Spatially uniform SOS activity in SMs disrupts cell migration and cytoskeletal organization. (A) Schematic of native SOS-1 localization in a migrating SM (see Figure 4A) contrasted with spatially uniform SOS activity caused by constitutively membrane-associated *Phlh8*>SOS^{cat}::2x mT2::PH. **(B)** Representative, live spinning disk confocal image showing migration defect caused by *Phlh8*>SOS^{cat}::2x mT2::PH in a wild-type background. The SM (arrow) failed to migrate and is dorsally displaced. **(C)** Representative, live spinning disk confocal images of SM positions at the end of migration in *egl-17(Δ); Pegl-20>FGF/egl-17* and *Phlh8*>SOS^{cat}::2x mT2::PH; *egl-17(Δ); Pegl-20>FGF/egl-17* animals. Expressing *FGF/egl-17* in the tail normally reorients SMs to migrate posteriorly in an *egl-17(Δ)* background. This migration is suppressed by *Phlh8*>SOS^{cat}::2x mT2::PH. Dashed white arrow denotes the migratory path taken by the SM. **(D)** Representative, live spinning disk confocal images showing SM positioning in a *Phlh8*>SOS^{cat}::2x mT2::PH; mNG::AID::ERK/MPK-1 animal where endogenous ERK/MPK-1 was depleted in the M lineage. Depleting ERK/MPK-1 suppressed the dorsoventral defects caused by membrane-associated SOS^{cat} and enhanced the anteroposterior migration defect. **(E)** Dot plot summarizing SM positioning in animals expressing SOS^{cat}::2x mT2::PH in the M lineage in different genetic backgrounds. Area of each dot is proportional to the frequency of cells stopping at that position. Asterisks indicate statistical significance for indicated comparisons (Fisher's exact test, * indicates $p<0.05$, *** indicates $p<0.0005$). $n\geq60$ for all strains. Source data available in Table S1. (**F**) Representative, live spinning disk confocal images showing actin organization in migrating SMs visualized by *2x mKate2::moesin* in wild-type and *Phlh8*>SOS^{cat}::2x mT2::PH animals. White arrows indicate actin enrichment at the leading edge in a wild type animal and disorganized throughout the cell in a *Phlh8*>SOS^{cat}::2x mT2::PH animal. White triangles in B, C, and D indicate the normal endpoint of SM migration.

Circular objects visible in both fluorescence channels are autofluorescent gut granules. All images are oriented with anterior to left and dorsal to top. Scale bars = 10μm.

Figure 5. Cell type-specific Ras gain of function and an intragenic revertant mutation suggest permissive roles for Ras/LET-60 in SM migration and distinct Ras signal transduction mechanisms in SMs and VPCs. (A) Representative, live spinning disk confocal images of final SM positioning in wild type and *FGFR/egl-15(n1458)* animals with activated *Ras/let-60(G13E)* expressed in the M lineage. **(B)** Schematic diagram showing alignment of human K-Ras and *C. elegans* LET-60 with the G13E (gain of function) and G75D (intragenic revertant) mutations emphasized. **(C)** Dot plot summarizing SM migration endpoints in strains used to dissect roles for activated *Ras*/*let-60* signaling in SM migration. Area of each dot is proportional to the frequency of cells stopping at that position. Asterisks indicate statistical significance for indicated comparisons (Fisher's exact test, * indicates $p<0.05$, *** indicates $p<0.0005$). $n\geq60$ for all strains shown. Source data available in Table S1. **(D)** Representative, live spinning disk confocal images showing young adult morphology and the stopping position of the SM in an L3 animal in a *Ras/let-60(G13E)* background. Arrows indicate the multivulval phenotype characteristic of Ras/ERK gain of function in VPCs. (**E**) Representative, live spinning disk confocal images showing L4 morphology and the stopping position of the SM in an L3 animal in a *Ras/let-60(G13E G75D)* background. *Ras/let-60(G13E G75D)* suppresses the multivulval phenotype caused by *Ras/let-60(G13E)* but leads to SM migration defects. White triangles indicate the normal endpoint of migration in A, D, and E. Small, circular objects visible in the fluorescence channel are autofluorescent gut granules. All images are oriented with anterior to left and dorsal to top. Scale bars = 10μm.

Figure 6. Depleting key cytoskeletal regulators leads to M lineage defects but does not affect migration. (A) Schematic of SM divisions and normal morphology at the 1-, 2-, and 8-SM stages. SMs proliferate after completing their migration. **(B)** Spinning disk confocal images of a 2 SM stage animal showing abnormally oriented cell division caused by CED-10/MIG-2 depletion. **(C)** Live spinning disk confocal images of a 1 SM stage animal showing a second, ectopic SM caused by WVE-1+WSP-1 depletion. **(D)** Live spinning disk confocal images of animals at the 8 SM stage showing SM division and/or differentiation defects caused by ARX-2, WVE-1, or WVE-1+WSP-1 depletion. We frequently observed additional SM cells along with dorsally and posteriorly displaced SMs (arrows). Note the total number of SMs at the 8 SM stage is not always divisible by 2, indicating potential loss of SM fate in some progeny, failures to follow normal cell division patterns, or presence of ectopic SMs. **(E)** Dot plot summarizing SM migration endpoints after M-lineage specific depletion of endogenously tagged proteins or in mutant strains. Area of each dot is proportional to the frequency of cells stopping at that position. Asterisks indicate statistical significance compared to wild-type animals (Fisher's exact test, * indicates $p<0.05$, ** indicates $p<0.005$). Data plotted for CED-10/MIG-2, ARX-2, WVE-1, and WVE-1/WSP-1 depletion are from animals with timed depletion and scored at the 1 SM stage. $n\geq60$ for all strains shown. Source data for continuous and timed depletion experiments are available in Table S1. White triangles indicate the normal endpoint of SM migration. Small, circular objects visible in both fluorescence channels are autofluorescent gut granules. All images are oriented with anterior to left and dorsal to top. Scale bars = 10μm.

Video 1. mNG::AID::SOS-1 localizes to dynamic punctae in leading edge protrusions during SM migration. Time-lapse imaging of endogenously tagged mNG::AID::SOS-1 in a migrating SM. Video corresponds to still images in Figure 4B. Anterior is to left and dorsal to top. Images were acquired at 1 minute intervals. https://doi.org/10.6084/m9.figshare.28780973.v1

Supplemental Information

Document S1. Includes Figures S1 – S9; Tables S1 and S2; Resources and Reagents table; Supplemental File 1

Video S1. Related to Figure S7.

Document S1 includes:

Figure S1. Diagram of the methodology for scoring SM positions using M lineage-derived body wall muscles as reference points. (A) Diagram of positions used for scoring SM positions relative to the M lineage-derived body wall muscle cells on the ventral side. Image shows average cell positioning in an *FGFR/egl-15(n1458)* mutant with impaired SM migration. For simplicity, only the left side of the worm is shown. Cells were scored based on where the cell body was positioned relative to the M-derived body wall muscle cells. We referred to the most anterior, M-derived, ventral body wall muscle cell as v17, whose anterior limit overlaps P6.p. For cells migrating posteriorly to category 4, the v20 or v22 cell was used as a reference (the most anterior of the two posterior ventral body wall cells on either the left or right respectively). The grey asterisk indicates the normal birthplace of SMs, with the curved dashed grey arrow indicating the distance the SMs normally travel even in the absence of FGF (EGL-17) or FGFR (EGL-15). Black triangle indicates normal endpoint of migration, above the vulval precursor cell (P6.p). **(B)** Example image of SM at a stopping position score of 3 in an *FGFR/egl-15(n1458)* background. White triangle indicates the normal endpoint of migration. **(C)** Diagram of M lineage divisions that from late L1 to the late L2 stage. CC= Coelomocyte, BWM = Body Wall Muscle, SM = Sex Myoblast, d= dorsal, v = ventral, l = left, r = right, a = anterior, p = posterior. BWM in red indicates cells that were used as references to score SM positions (v17, v20, v22). Scale bar = 10μm.

Figure S2. *ksr-1*, *age-1*, *plc-3*, and *abl-1* mutants do not have SM migration defects. (A) Representative, live spinning disk confocal image showing SM positioning in a *ksr-1(n2526)* mutant animal. **(B)** Schematic of *ksr-1* mutants used here *(n2526)* and previously described (*ku68*) and (*ku83*). **(C)** Live spinning disk confocal images showing SM positioning in an *age-1(m333)* background. The left image is representative of the majority of animals. The right image shows an animal with an extra SM (arrow), which is indicative of an earlier M lineage defect. **(D)** Representative, live spinning disk confocal image showing SM positioning in a *plc-3(tm1340)* animal. *plc-3(tm1340)* homozygous animals were picked for imaging by the absence of a *dpy* phenotype or the pharyngeal GFP signal that marks the balancer chromosome in the parental strain. **(E)** Representative, live spinning disk confocal image showing SM positioning in an *abl-1(ok171)* background. White triangles indicate the normal endpoint of migration in A, C-

E. Small, circular objects visible in fluorescence channels are autofluorescent gut granules. All images are oriented with anterior to left and dorsal to top. Scale bars = 10μm.

Figure S3. Depleting ERK/MPK-1 in the M lineage results in elongated SMs but does not affect migration. (A) Representative, live spinning disk confocal image showing an abnormally elongated SM that is located in the correct final position above P6.p after mNG::AID::ERK/MPK-1 depletion. White triangles indicate the normal endpoint of migration. Circular objects visible in both fluorescence channels are autofluorescent gut granules. All images are oriented with anterior to left and dorsal to top. Scale bars = 10μm.

Figure S4. Membrane-associated GRB2/SEM-5 activity disrupts SM migration. (A) Schematic of the GRB2/SEM-5::PH::mNG construct with the SH2 domain replaced with the PH domain for *plc1δ1* used to mislocalize the SOS catalytic domain. **(B)** Dot plot summarizing SM migration endpoints with membrane-associated SOS^{cat} or GRB2/SEM-5. Area of each dot is proportional to the frequency of cells stopping at that position. Asterisks indicate statistical significance compared to wild-type animals (Fisher's exact test, *** indicates $p<0.0005$). $n\geq60$ for all strains shown. Source data available in Table S1. **(C)** Live spinning disk confocal image showing SEM-5::PH::mNG localization. Note the non-uniform localization of the fusion protein. White triangle indicates the normal endpoint of migration. All images are oriented with anterior to left and dorsal to top. Scale bars = 10μm.

Figure S5. ERK/MPK-1 depletion suppresses dorsal and enhances anterior migration defects in a *Phlh8>Ras/let-60(G13E); FGFR/egl-15(n1458)* background. (A) Live spinning disk confocal image showing a dorsally displaced SM in a *Phlh8>Ras/let-60(G13E); FGFR/egl-15(n1458)* animal. Note the cell migrated anteriorly to the correct position but is dorsally displaced. **(B)** Representative, live spinning disk confocal images of a K-NAA-treated mNG::AID::ERK/MPK-1; *Phlh8>Ras/let-60(G13E); FGFR/egl-15(n1458)* worm. White triangles indicate the normal endpoint of migration. All images are oriented with anterior to left and dorsal to top. Scale bars = 10μm.

Figure S6. Identification of the molecular lesion responsible for *let-60(n1046ku75)*. Sanger sequencing gel showing DNA sequences of *let-60* PCR products in *let-60(n1046)* and *let-60(n1046ku75)* animals. *ku75* is G>A nucleotide substitution that leads to a glycine to aspartic acid substitution at amino acid position 75.

Figure S7: Ras/LET-60(G75D) substitution is predicted to perturb interactions between Ras/LET-60 and SOS-1. Ras/LET-60(G75D) is predicted to displace the Ras/LET-60 α helix 2 that interacts with SOS proteins, thus perturbing predicted interactions. **A**-**E**) PyMOL visualization of a crystal structure (PDB: 8EBZ) of human KRas G13D with GMPPNP non-hydrolyzable GTP analog (without the C-terminal hypervariable (HVR)+CAAX membrane-targeting sequences). Color coding. Small GTPase = pale green, nucleotide = salmon, basic charges = dark blue, acidic charges = red, Mg^{2+} = pale cyan, G1-5 boxes that coordinate nucleotide binding = yellow, core effector binding loop = lavender, residue 13 = bright green, residue 75 = lt. blue, residue 7 = gray, last residue of the GTPase domain = red and is oriented

upwards where it would normally extend to the HVR+CAAX sequences and the lipid bilayer. (**A**, **B**) Without the R-group to illustrate Gly13 vs. G13E. The structure (PDB: 8EBZ) is for KRas G13D, but Glutamate13 was substituted for Aspartate here to illustrate the *C. elegans let-60(n1046*gf[G13E]*)* mutant. The Asp13 changes causes mild constitutive loading of KRas, and Glu13 is expected to be similar. (**C**) Position of the G75D mutant change caused by the *Ras/let-60(n1046 ku75 [G13E G75D])* intragenic revertant mutation. (D-E) Zoomed in views contrasting wild-type Gly75 and mutant G75D. (**D**) The single H+ atom of the Gly75 side chain (not depicted) does not conflict with Val7, shown in gray (F78 not highlighted). (**E**) The larger and acidic G75D side chain is predicted to conflict with V7 in the hydrophobic core. This and steric interference are expected to displace the neighboring α helix 2. (**F-H**) PyMOL visualization of predicted interactions between KRas(G13E G75D) and SOS based on the crystal structure of a human ternary KRas(G13D)-SOS complex (PDB: 7KFZ). Color coding: Human SOS1: REM = blue, GEF = teal, other sequences pale cyan. KRas(G13D): GTPase = pale green, GTP = salmon, Mg^{2+} = pale cyan, G boxes coordinating nucleotide binding = yellow, basic charges = dark blue, acidic charges = red, N- and C-terminal residues = red, alpha helix 2 residues oriented toward SOS = pink. (**F**) View of two KRas molecules bound to the SOS allosteric and catalytic sites. Dashed boxes show locations of zoomed views in G and H. (**G**) Zoomed view of predicted interaction between KRas-GTP(G75D) and the REM domain of SOS1 at its allosteric Ras-binding site. Gly75, altered by the G75D mutation, is shown as mutant Aspartate that interferes with Val7 and Phe78 with side chain. Dark blue = basic, red = acidic, yellow = sulfur. (**H**) Zoomed view of predicted interaction between apoKRas(G75) and the CDC25/GEF domain of SOS1 at its catalytic site.

Figure S8. Key cytoskeletal regulators are not required cell autonomously for SM migration. (A) Representative, live spinning disk confocal images showing SM positioning and localization of endogenously tagged proteins in control and K-NAA-treated animals. SMs are outlined in yellow in single channel images of tagged endogenous proteins, and white triangles denote the normal endpoint of SM migration. Fluorescence remaining within the yellow outline in images of K-NAA treated worms is due to high expression in underlying somatic gonad cells, which cannot be separated by confocal microscopy due to their proximity in the Z-plane. The small, circular objects visible in both fluorescence channels are autofluorescent gut granules. All images are oriented with anterior to left and dorsal to top. Scale bars = 10μm.

Figure S9. Relative expression of targeted candidates genes in SMs in L2 scRNAseq data. (A) Relative gene expression frequency[44] for the sixteen genes targeted by auxin-inducible degradation. Note that we observed strong SM migration defects when targeting the 3 highest-expressed genes.

Video S1. Ras/LET-60(G75D) substitution is predicted to perturb interactions between Ras/LET-60 and SOS-1. Video shows rotated views of predicted interactions between KRas(G13E G75D) and SOS based on the crystal structure of a human ternary KRas(G13D)-SOS complex (PDB: 7KFZ). See Figure S7 for annotations. https://doi.org/10.6084/m9.figshare.28780997.v1

Table S1. Source data for SM positioning.

Table S2. An intragenic revertant of *let-60(n1046gf)* causes strong SM migration defects

Supplemental File 1: Genome editing and molecular cloning information

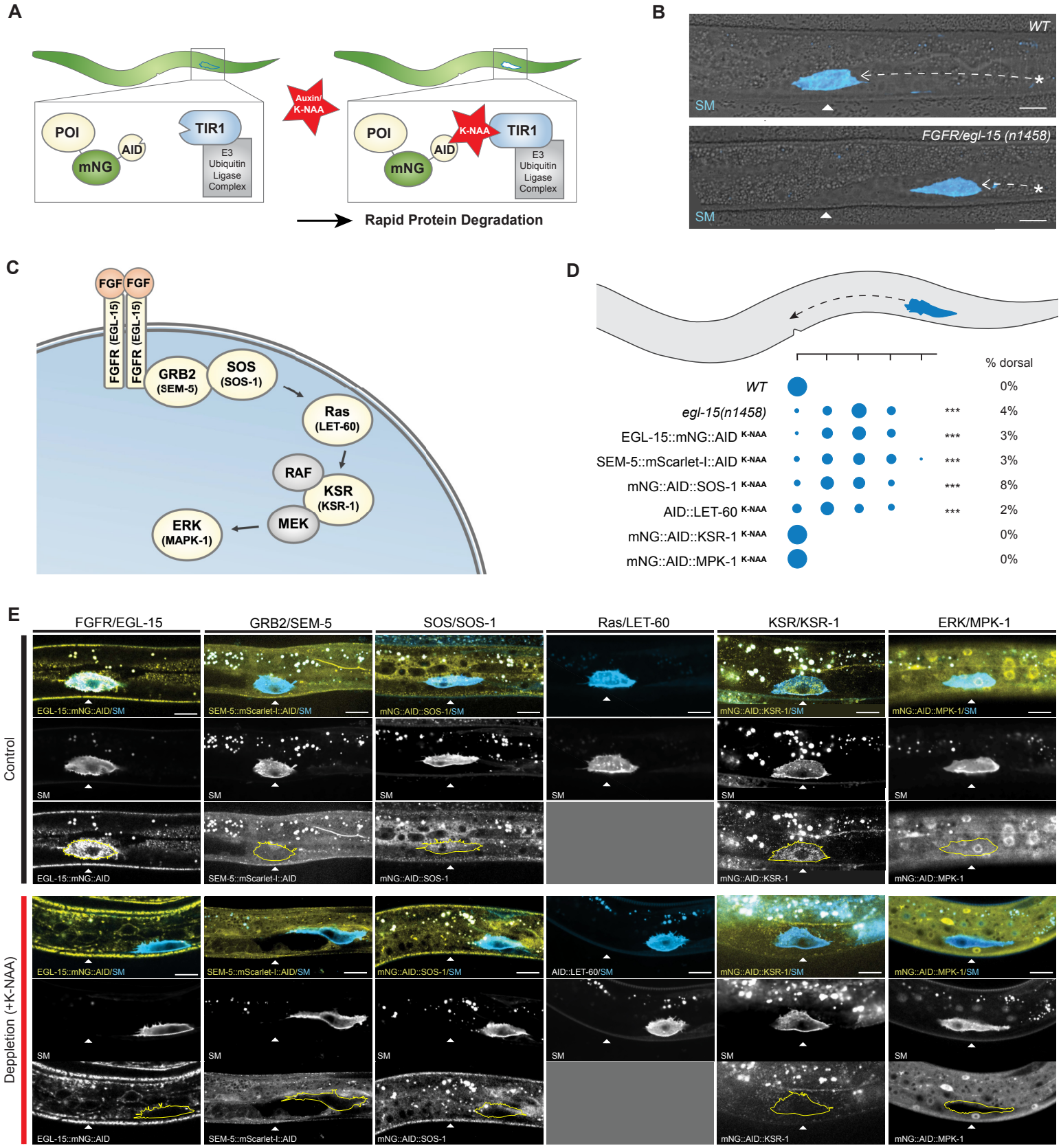
A
POI
AID
mNG
TIR1
E3 Ubiquitin Ligase Complex
Auxin/ K-NAA
K-NAA
Rapid Protein Degradation
B
WT
SM
FGFR/egl-15 (n1458)
C
FGF
FGFR (EGL-15)
GRB2 (SEM-5)
SOS (SOS-1)
Ras (LET-60)
RAF
KSR (KSR-1)
MEK
ERK (MAPK-1)
D
% dorsal
WT 0%
egl-15(n1458) *** 4%
EGL-15::mNG::AID K-NAA *** 3%
SEM-5::mScarlet-I::AID K-NAA *** 3%
mNG::AID::SOS-1 K-NAA *** 8%
AID::LET-60 K-NAA *** 2%
mNG::AID::KSR-1 K-NAA 0%
mNG::AID::MPK-1 K-NAA 0%
E
FGFR/EGL-15
GRB2/SEM-5
SOS/SOS-1
Ras/LET-60
KSR/KSR-1
ERK/MPK-1
Control
Deppletion (+K-NAA)
EGL-15::mNG::AID/SM
SEM-5::mScarlet-I::AID/SM
mNG::AID::SOS-1/SM
mNG::AID::KSR-1/SM
mNG::AID::MPK-1/SM
AID::LET-60/SM
SM
EGL-15::mNG::AID
SEM-5::mScarlet-I::AID
mNG::AID::SOS-1
mNG::AID::KSR-1
mNG::AID::MPK-1

Figure 1

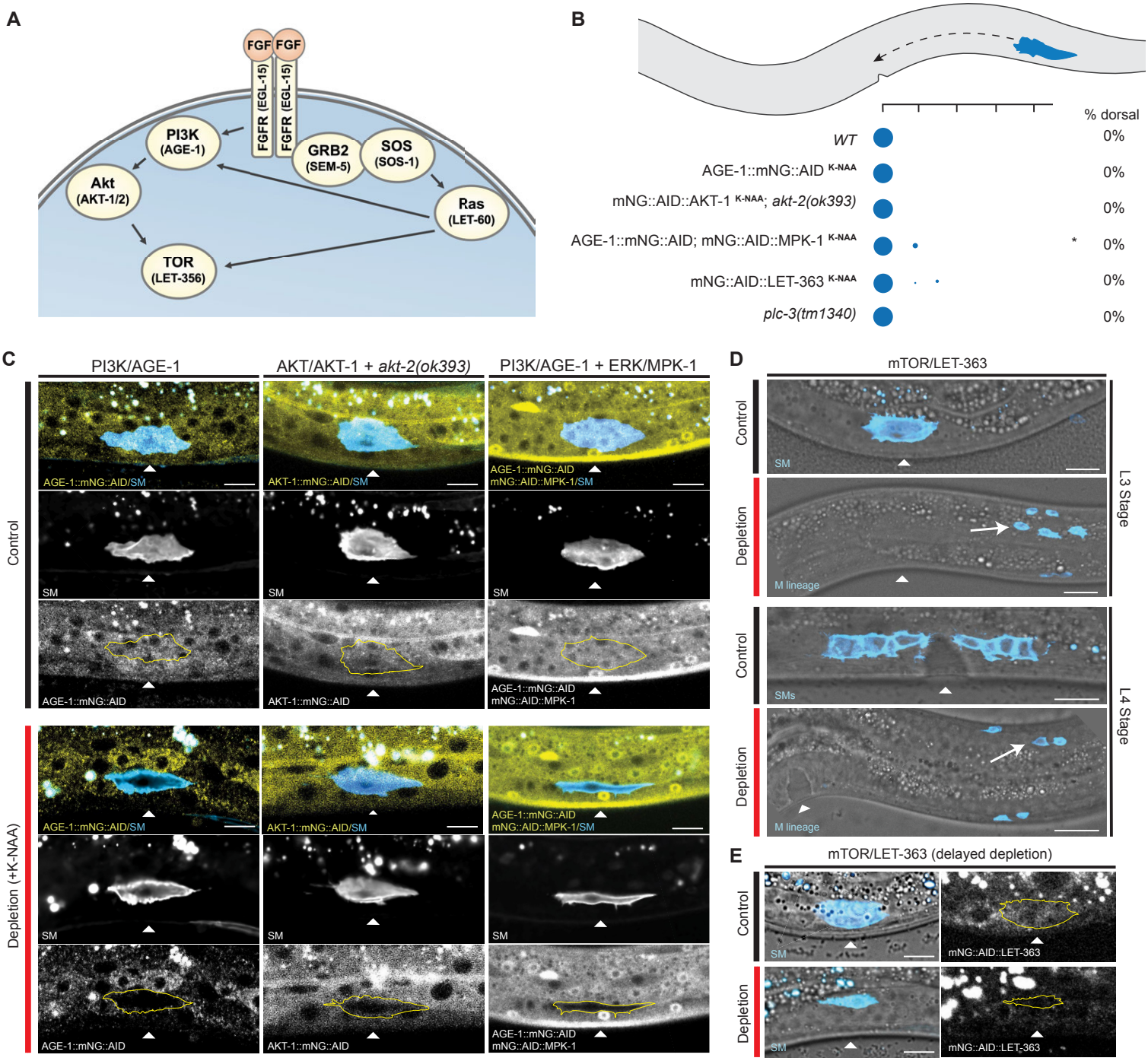
A
FGF
FGF
FGFR (EGL-15)
FGFR (EGL-15)
PI3K (AGE-1)
GRB2 (SEM-5)
SOS (SOS-1)
Akt (AKT-1/2)
Ras (LET-60)
TOR (LET-356)
B
% dorsal
WT 0%
AGE-1::mNG::AID K-NAA 0%
mNG::AID::AKT-1 K-NAA; akt-2(ok393) 0%
AGE-1::mNG::AID; mNG::AID::MPK-1 K-NAA * 0%
mNG::AID::LET-363 K-NAA 0%
plc-3(tm1340) 0%
C
PI3K/AGE-1
AKT/AKT-1 + akt-2(ok393)
PI3K/AGE-1 + ERK/MPK-1
Control
Depletion (+K-NAA)
AGE-1::mNG::AID/SM
AKT-1::mNG::AID/SM
AGE-1::mNG::AID mNG::AID::MPK-1/SM
SM
AGE-1::mNG::AID
AKT-1::mNG::AID
AGE-1::mNG::AID mNG::AID::MPK-1
D
mTOR/LET-363
Control
Depletion
L3 Stage
L4 Stage
SM
M lineage
SMs
E
mTOR/LET-363 (delayed depletion)
mNG::AID::LET-363

Figure 2

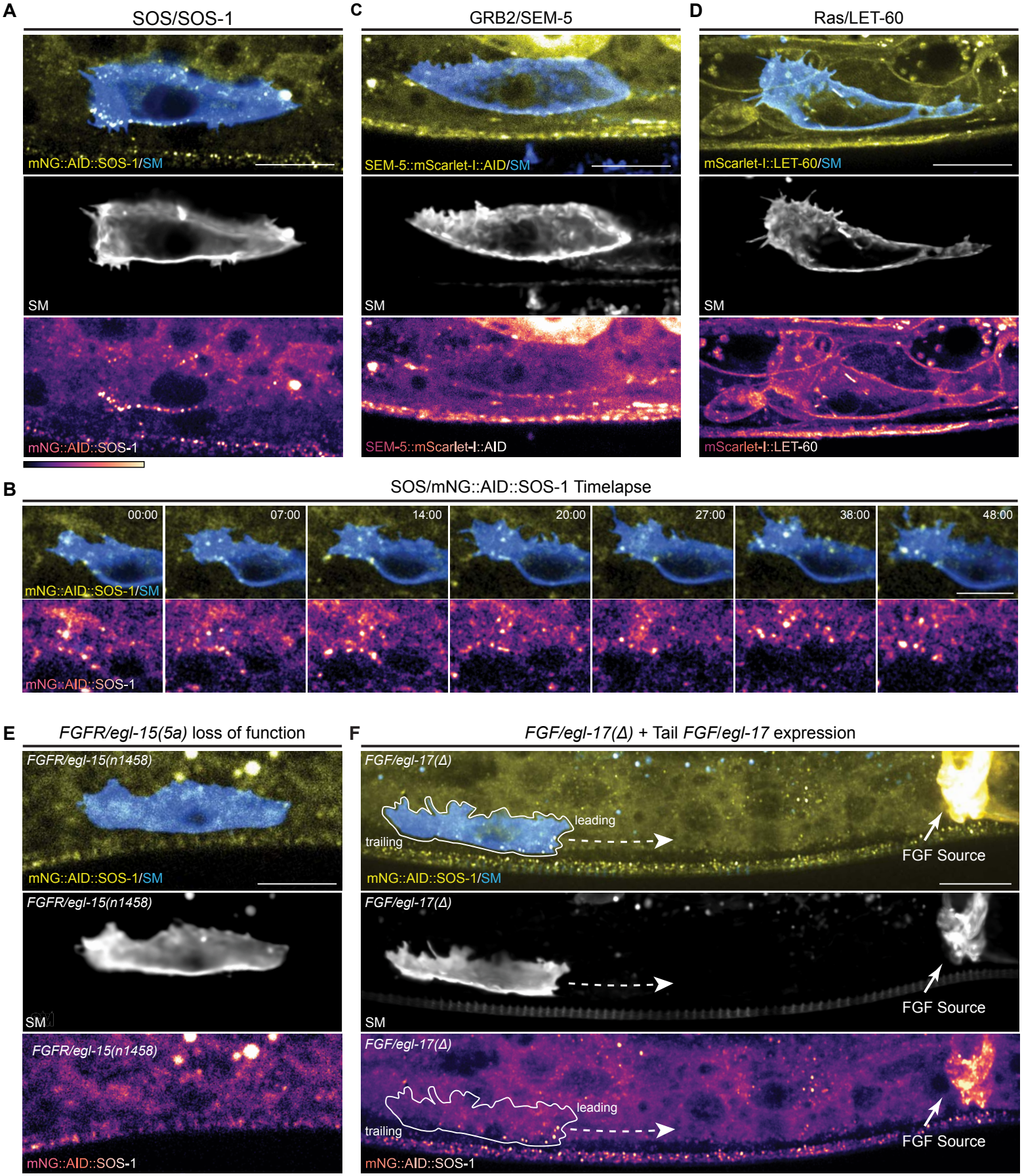
A
SOS/SOS-1
mNG::AID::SOS-1/SM
SM
mNG::AID::SOS-1
C
GRB2/SEM-5
SEM-5::mScarlet-I::AID/SM
SM
SEM-5::mScarlet-I::AID
D
Ras/LET-60
mScarlet-I::LET-60/SM
SM
mScarlet-I::LET-60
B
SOS/mNG::AID::SOS-1 Timelapse
00:00
07:00
14:00
20:00
27:00
38:00
48:00
mNG::AID::SOS-1/SM
mNG::AID::SOS-1
E
FGFR/egl-15(5a) loss of function
FGFR/egl-15(n1458)
mNG::AID::SOS-1/SM
FGFR/egl-15(n1458)
SM
FGFR/egl-15(n1458)
mNG::AID::SOS-1
F
FGF/egl-17(Δ) + Tail FGF/egl-17 expression
FGF/egl-17(Δ)
leading
trailing
FGF Source
mNG::AID::SOS-1/SM
FGF/egl-17(Δ)
FGF Source
SM
FGF/egl-17(Δ)
leading
trailing
FGF Source
mNG::AID::SOS-1

Figure 3

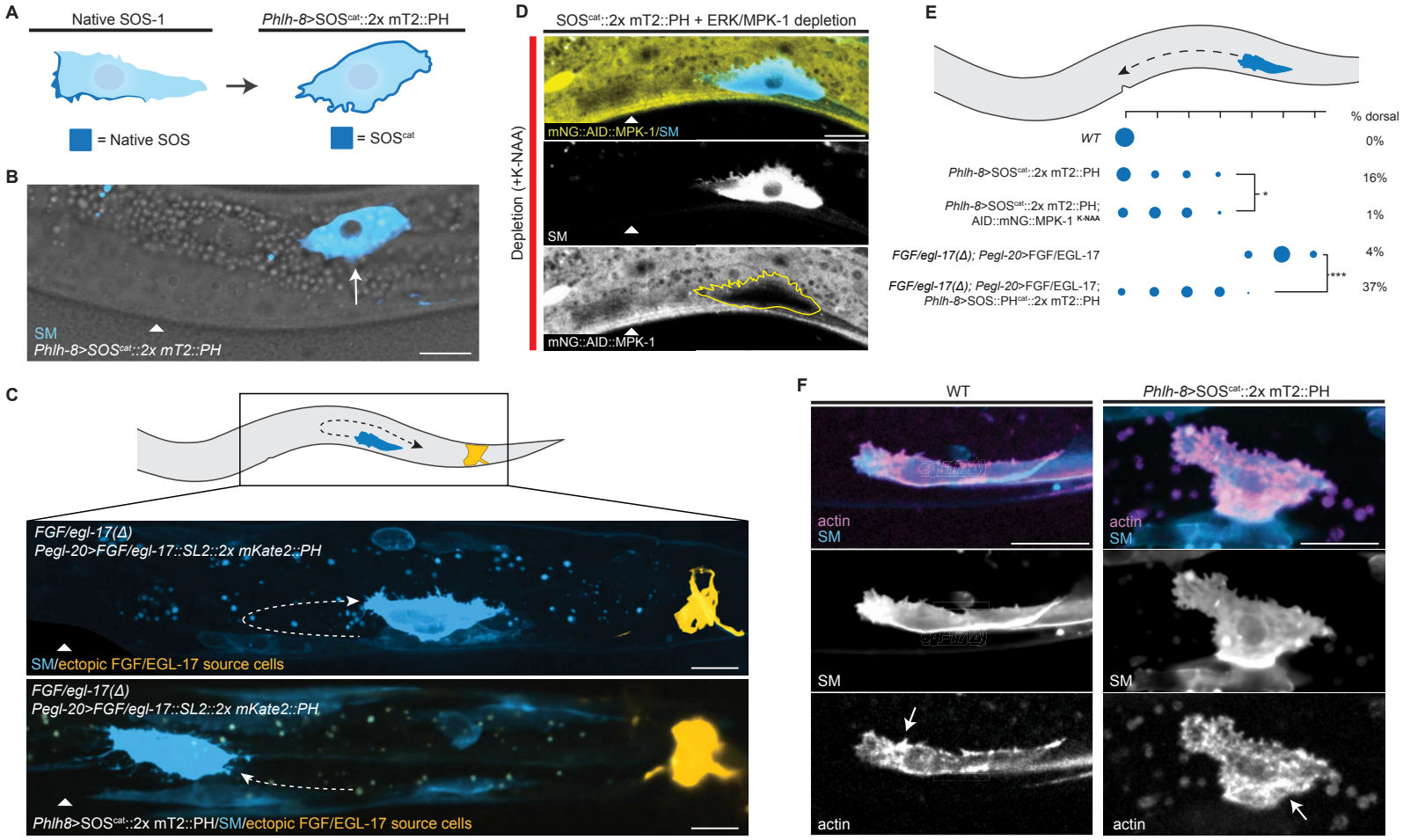
A
Native SOS-1
Phlh-8>SOS^cat::2x mT2::PH
= Native SOS
= SOS^cat
B
SM
Phlh-8>SOS^cat::2x mT2::PH
C
FGF/egl-17(Δ)
Pegl-20>FGF/egl-17::SL2::2x mKate2::PH
SM/ectopic FGF/EGL-17 source cells
FGF/egl-17(Δ)
Pegl-20>FGF/egl-17::SL2::2x mKate2::PH
Phlh8>SOS^cat::2x mT2::PH/SM/ectopic FGF/EGL-17 source cells
D
SOS^cat::2x mT2::PH + ERK/MPK-1 depletion
Depletion (+K-NAA)
mNG::AID::MPK-1/SM
SM
mNG::AID::MPK-1
E
% dorsal
WT
0%
Phlh-8>SOS^cat::2x mT2::PH
16%
Phlh-8>SOS^cat::2x mT2::PH;
AID::mNG::MPK-1 K-NAA
1%
FGF/egl-17(Δ); Pegl-20>FGF/EGL-17
4%
FGF/egl-17(Δ); Pegl-20>FGF/EGL-17;
Phlh-8>SOS::PH^cat::2x mT2::PH
37%
F
WT
Phlh-8>SOS^cat::2x mT2::PH
actin
SM
SM
actin

Figure 4

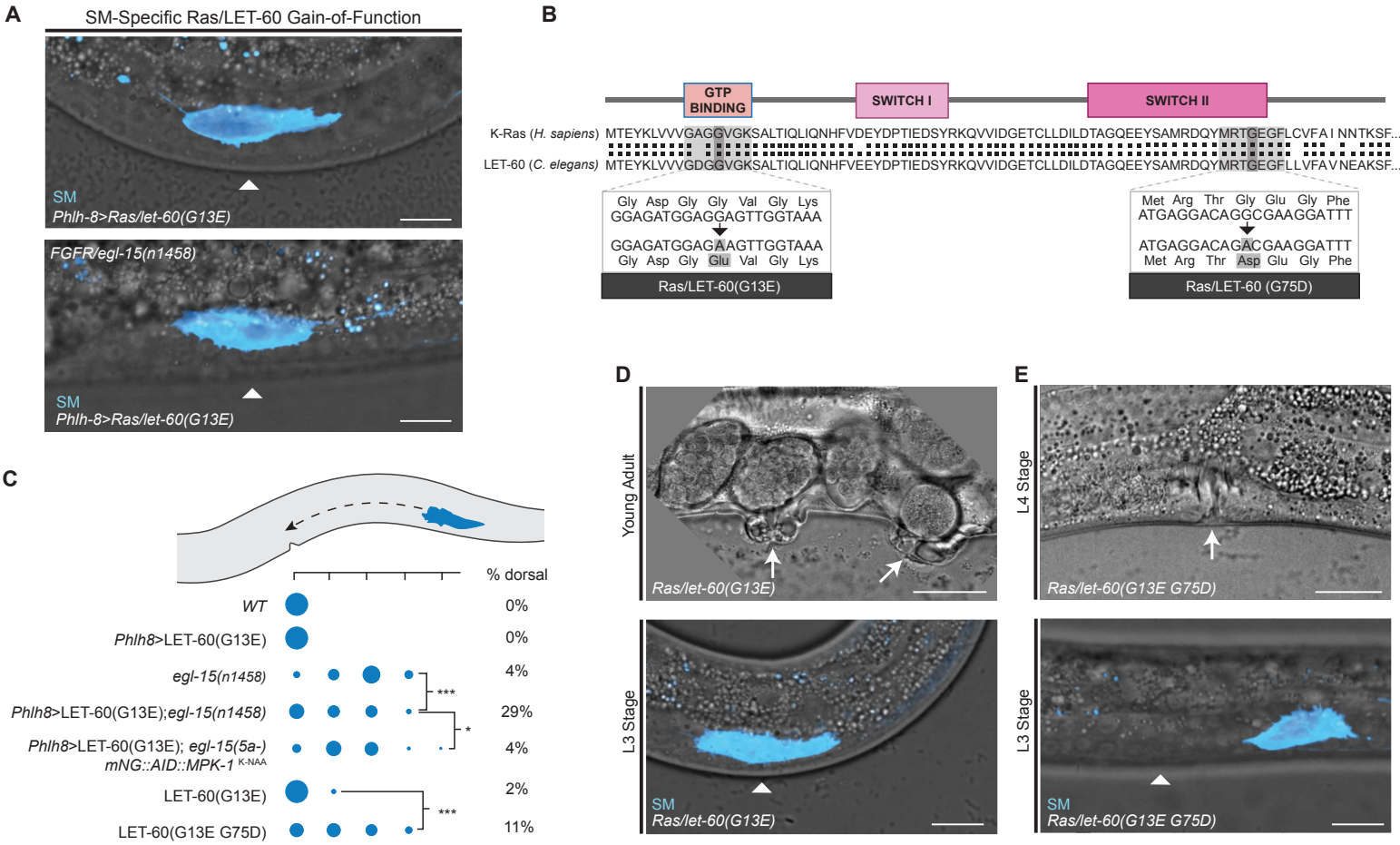
A
SM-Specific Ras/LET-60 Gain-of-Function
SM
Phlh-8>Ras/let-60(G13E)
FGFR/egl-15(n1458)
SM
Phlh-8>Ras/let-60(G13E)
B
GTP BINDING
SWITCH I
SWITCH II
K-Ras (H. sapiens) MTEYKLVVVGAGGVGKSALTIQLIQNHFVDEYDPTIEDSYRKQVVIDGETCLLDILDTAGQEEYSAMRDQYMRTGEGFLCVFAINNTKSF...
LET-60 (C. elegans) MTEYKLVVVGDGGVGKSALTIQLIQNHFVEEYDPTIEDSYRKQVVIDGETCLLDILDTAGQEEYSAMRDQYMRTGEGFLLVFAVNEAKSF...
Gly Asp Gly Gly Val Gly Lys
GGAGATGGAGGAGTTGGTAAA
GGAGATGGAGAAGTTGGTAAA
Gly Asp Gly Glu Val Gly Lys
Ras/LET-60(G13E)
Met Arg Thr Gly Glu Gly Phe
ATGAGGACAGGCGAAGGATTT
ATGAGGACAGACGAAGGATTT
Met Arg Thr Asp Glu Gly Phe
Ras/LET-60 (G75D)
C
% dorsal
WT 0%
Phlh8>LET-60(G13E) 0%
egl-15(n1458) 4%
***
Phlh8>LET-60(G13E);egl-15(n1458) 29%
*
Phlh8>LET-60(G13E); egl-15(5a-) mNG::AID::MPK-1 K-NAA 4%
LET-60(G13E) 2%
***
LET-60(G13E G75D) 11%
D
Young Adult
Ras/let-60(G13E)
L3 Stage
SM
Ras/let-60(G13E)
E
L4 Stage
Ras/let-60(G13E G75D)
L3 Stage
SM
Ras/let-60(G13E G75D)

Figure 5

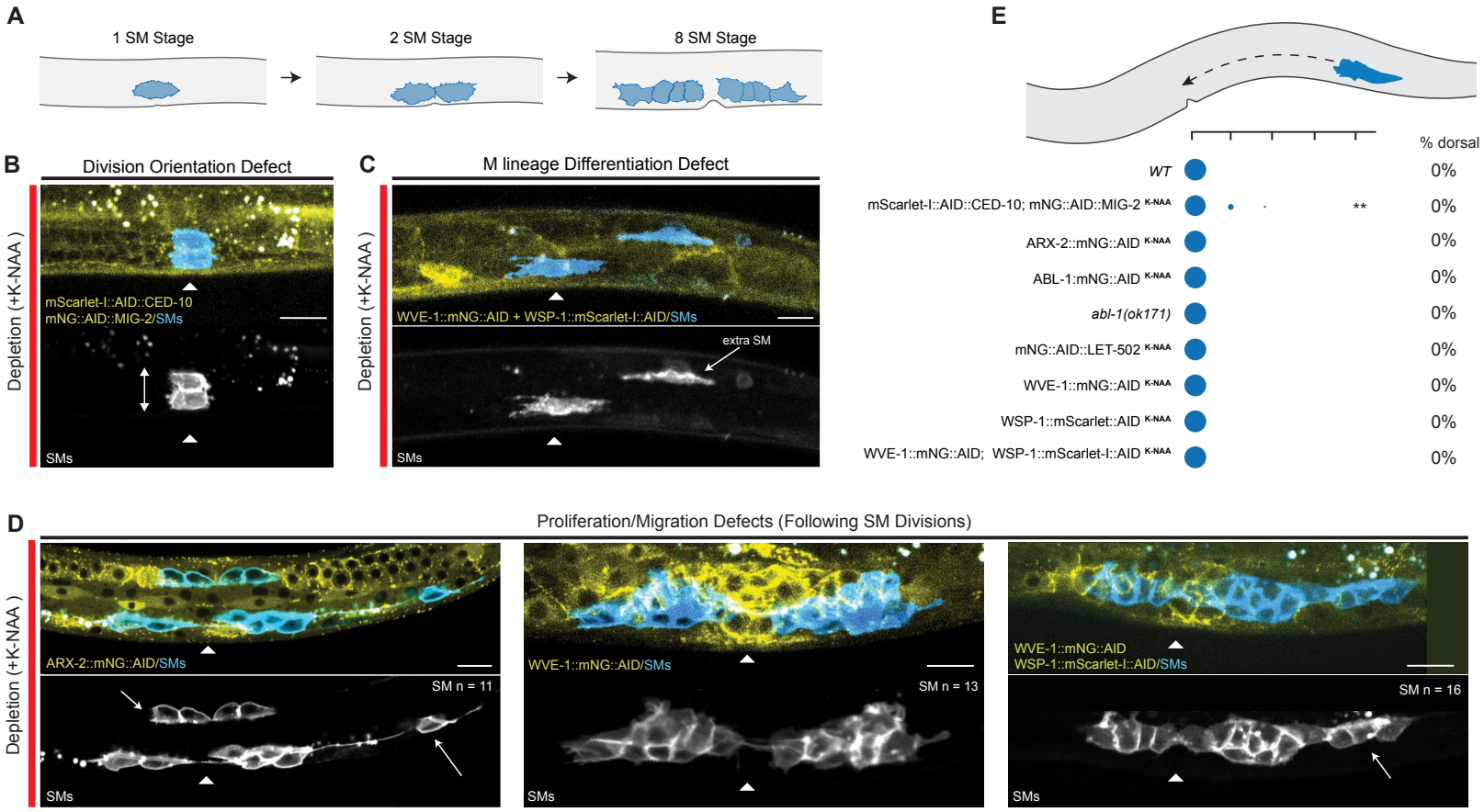
A
1 SM Stage
2 SM Stage
8 SM Stage
B
Division Orientation Defect
Depletion (+K-NAA)
mScarlet-I::AID::CED-10
mNG::AID::MIG-2/SMs
SMs
C
M lineage Differentiation Defect
Depletion (+K-NAA)
WVE-1::mNG::AID + WSP-1::mScarlet-I::AID/SMs
extra SM
SMs
E
% dorsal
WT
0%
mScarlet-I::AID::CED-10; mNG::AID::MIG-2 K-NAA
**
0%
ARX-2::mNG::AID K-NAA
0%
ABL-1::mNG::AID K-NAA
0%
abl-1(ok171)
0%
mNG::AID::LET-502 K-NAA
0%
WVE-1::mNG::AID K-NAA
0%
WSP-1::mScarlet::AID K-NAA
0%
WVE-1::mNG::AID; WSP-1::mScarlet-I::AID K-NAA
0%
D
Proliferation/Migration Defects (Following SM Divisions)
Depletion (+K-NAA)
ARX-2::mNG::AID/SMs
SM n = 11
SMs
WVE-1::mNG::AID/SMs
SM n = 13
SMs
WVE-1::mNG::AID
WSP-1::mScarlet-I::AID/SMs
SM n = 16
SMs

Figure 6